

INFERRING INTERWELL CONNECTIVITY IN A RESERVOIR FROM BOTTOMHOLE PRESSURE FLUCTUATIONS OF HYDRAULICALLY FRACTURED VERTICAL WELLS, HORIZONTAL WELLS, AND MIXED WELLBORE CONDITIONS

Dinh Viet Anh¹, Djebbar Tiab²

¹PetroVietnam Exploration Production Corporation

²University of Oklahoma

Email: anhdv@pvep.com.vn; dtiab@ou.edu

<https://doi.org/10.47800/PVJ.2020.10-03>

Summary

A technique using interwell connectivity is proposed to characterise complex reservoir systems and provide highly detailed information about permeability trends, channels, and barriers in a reservoir. The technique, which uses constrained multivariate linear regression analysis and pseudosteady state solutions of pressure distribution in a closed system, requires a system of signal (or active) wells and response (or observation) wells. Signal wells and response wells can be either producers or injectors. The response well can also be either flowing or shut in. In this study, for consistency, waterflood systems are used where the signal wells are injectors, and the response wells are producers. Different borehole conditions, such as hydraulically fractured vertical wells, horizontal wells, and mixed borehole conditions, are considered in this paper.

Multivariate linear regression analysis was used to determine interwell connectivity coefficients from bottomhole pressure data. Pseudosteady state solutions for a vertical well, a well with fully penetrating vertical fractures, and a horizontal well in a closed rectangular reservoir were used to calculate the relative interwell permeability. The results were then used to obtain information on reservoir anisotropy, high-permeability channels, and transmissibility barriers. The cases of hydraulically fractured wells with different fracture half-lengths, horizontal wells with different lateral section lengths, and different lateral directions are also considered. Different synthetic reservoir simulation models are analysed, including homogeneous reservoirs, anisotropic reservoirs, high-permeability-channel reservoirs, partially sealing barriers, and sealing barriers.

The main conclusions drawn from this study include: (a) The interwell connectivity determination technique using bottomhole pressure fluctuations can be applied to waterflooded reservoirs that are being depleted by a combination of wells (e.g. hydraulically fractured vertical wells and horizontal wells); (b) Wellbore conditions at the observations wells do not affect interwell connectivity results; and (c) The complex pressure distribution caused by a horizontal well or a hydraulically fractured vertical well can be diagnosed using the pseudosteady state solution and, thus, its connectivity with other wells can be interpreted.

Key words: Interwell connectivity, bottomhole pressure fluctuations, waterflooding, vertical wells, horizontal wells, hydraulically fractured wells.

1. Introduction

Numerous studies on inferring interwell connectivity in a waterflood have been carried out. Some of these studies used statistical techniques that are very different

from the approach used in this study. Albertoni and Lake developed a technique that calculates the fraction of flow caused by each of the injectors in a producer [1, 2]. This method uses a constrained Multivariate Linear Regression (MLR) model similar to the model proposed by Refunjol [3]. The model introduced by Albertoni and Lake, however, considered only the effect of injectors on producers, not producers on producers. Albertoni and Lake also intro-



Date of receipt: 12/10/2020. Date of review and editing: 12 - 14/10/2020.

Date of approval: 15/10/2020.

This article was presented at SPE Production and Operations Symposium and licensed by SPE (License ID: 1068761-1) to republish full paper in Petrovietnam Journal

duced the concepts and uses of diffusivity filters to account for the time lag and attenuation that occur between the stimulus (injection) and the response (production). The procedures were proven effective for synthetic reservoir models, as well as real water flood fields. Yousef et al. introduced a capacitance model in which a nonlinear signal processing model was used [4, 5]. Compared to Albertoni and Lake's model which was a steady-state (purely resistive) one, the capacitance model included both capacitance (compressibility) and resistivity (transmissibility) effects. The model used flow rate data and could include shut-in periods and bottom hole pressures (if available).

Dinh and Tiab [6 - 9] used a similar approach as Albertoni and Lake [1, 2], however, bottom hole pressure data were used instead of flow rate data. Some constraints were applied to the flow rates such as constant production rate at every producer and constant total injection rate. Using bottom hole pressure data offers several advantages: (a) diffusivity filters are not needed, (b) minimal data is required and (c) flexible plan to collect data. All of the studies above only considered fully penetrating vertical wells. Dinh and Tiab only considered reservoirs with vertical wells without any hydraulic fractures or horizontal wells [6 - 9].

In this study, bottomhole pressure fluctuations were used to determine the interwell connectivity in a waterflood where horizontal wells, hydraulically fractured vertical wells or both are present. MLR model was used to determine the interwell connectivity coefficients from bottom-hole pressure data. For the case of hydraulically fractured vertical wells, a late time solution for a well with a fully penetrating vertical fracture in a closed rectangular reservoir was used to calculate the influence functions and the relative interwell permeabilities. The case where the fractures are of different fracture half-lengths is also considered. Similarly, for the horizontal well cases, the late time solution for a horizontal well in a closed rectangular reservoir was used to calculate the influence functions and the relative interwell permeabilities. The cases in which the reservoir contains horizontal wells of different lengths and different directions were also considered. In order to quantify the effect of observation wells on the interwell

connectivity coefficients, the case of different injector well lengths and unchanged producer well lengths was analysed. Results for different cases such as all wells are horizontal along the x-direction, along both x- and y-directions and different horizontal well lengths are provided.

This study also provides the results for different cases where mixed wellbore conditions are present. 5 injector and 4 producer synthetic reservoirs containing hydraulic fractures and vertical wells, horizontal and vertical wells or all three types of wellbore conditions are used in the analysis. The results were then used to obtain information on reservoir anisotropy, high permeability channels and transmissibility barriers. Different synthetic reservoir models were analysed including homogeneous, anisotropic reservoirs, reservoirs with high permeability channel, partially sealing barrier and sealing barrier.

2. Analytical model and calculation approach

Previous studies have developed a novel technique to determine interwell connectivity from bottom hole pressure fluctuation data. This study extends the application of the technique to hydraulically fractured, horizontal wells and mixed wellbore conditions. The technique was described in detail by Dinh and Tiab [6 - 9]. Key equations and definitions of dimensionless variables below are used throughout this study.

2.1. Dimensionless variable

Considering a multi-well system with producers or injectors and initial pressure p_i , the solution for pressure distribution due to a fully penetrated vertical well in a close rectangular reservoir is as follows [10, 11]:

$$p_D(x_D, y_D, t_{DA}) = \sum_{i=1}^{n_{well}} q_{D,i} a_i(x_D, y_D, x_{wD,i}, y_{wD,i}, x_{eD}, y_{eD}, [t_{DA} - t_{sDA}]) \quad (1)$$

Where the dimensionless variables are defined in field units as follows:

$$x_D = \frac{x}{\sqrt{A}} \quad (2)$$

$$y_D = \frac{y}{\sqrt{A}} \quad (3)$$

$$p_D = \frac{kh}{141.2q_{ref}B\mu} (p_{ini} - p(x, y, t)) \quad (4)$$

$$t_{DA} = 0.0002637 \frac{kt}{\phi c_t \mu A} \quad (5)$$

a_i is the influence function equivalent to the dimensionless pressure for the case of a single well in a bounded reservoir produced at a constant rate. Assuming $t_{sDA} = 0$, the influence function is given as:

$$\begin{aligned}
 & a_i(x_D, y_D, x_{wD,i}, y_{wD,i}, x_{eD}, y_{eD}, t_{DA}) \\
 &= \frac{1}{2} \sum_{m=-\infty}^{\infty} \sum_{n=-\infty}^{\infty} E_1 \left[\frac{(x_D + x_{wD,i} + 2nx_{eD})^2 + (y_D + y_{wD,i} + 2my_{eD})^2}{4t_{DA}} \right] \\
 &+ E_1 \left[\frac{(x_D - x_{wD,i} + 2nx_{eD})^2 + (y_D + y_{wD,i} + 2my_{eD})^2}{4t_{DA}} \right] \quad (6) \\
 &+ E_1 \left[\frac{(x_D + x_{wD,i} + 2nx_{eD})^2 + (y_D - y_{wD,i} + 2my_{eD})^2}{4t_{DA}} \right] \\
 &+ E_1 \left[\frac{(x_D - x_{wD,i} + 2nx_{eD})^2 + (y_D - y_{wD,i} + 2my_{eD})^2}{4t_{DA}} \right]
 \end{aligned}$$

Equation 6 is valid for pseudosteady state flow and can be rewritten as below:

$$p_{ini} - p(x, y) = \frac{141.2Bu}{kh} \sum_{i=1}^{n_{well}} a_n[x_D, y_D, x_{wDn}, y_{wDn}, x_{eD}, y_{eD}, t_{AD}] q_n \quad (7)$$

Equation 7 is the pressure response at point (x_D, y_D) due to a well n at (x_{wDn}, y_{wDn}) in a homogeneous closed rectangular reservoir. The influence function (a_n) can be different for different wellbore conditions as well as flow regimes (horizontal well, partial penetrating vertical well, fractured vertical well, etc.).

2.2. Shape factor calculation

Shape factors are used to calculate pressure at wells at different locations in a reservoir of a certain shape. Letting C_A denote the shape factor, we have the well known shape factor equation:

$$p_{wD} = 2\pi t_{DA} + 0.5 \ln \frac{4A}{e^\gamma C_A L^2} \quad (8)$$

with $L = r_w, L_{xf}$ and $L_h/2$ for vertical well, vertically fractured well and horizontal well respectively and γ is Euler's constant ($\gamma = 0.5772\dots$)

Thus, the shape factor can be calculated using Equation 9 [12]:

$$C_A = \text{Exp} \left[(4\pi t_{DA} - 2p_{wD}) + \text{Log} \frac{4A}{L^2 e^\gamma} \right] \quad (9)$$

Where the L term in the definitions of dimensionless quantities is $L = L_{xf}$ which is the fracture half-length.

2.3. Influence function

2.3.1. Hydraulically fractured well

For a hydraulically fractured well, for simplicity, the late time solution for a uniform flux fracture in

a closed rectangular reservoir provided by Ozkan was used [13]. The influence function for hydraulically fractured well becomes:

$$\begin{aligned}
 p_{Df} &= 2\pi t_{DA} + 2\pi \frac{y_{eD}}{x_{eD}} \left(\frac{1}{3} - \frac{y_D}{y_{eD}} + \frac{y_D^2 + y_{wD}^2}{2y_{eD}^2} \right) \\
 &+ \frac{2x_{eD}}{\pi} \sum_{k=1}^{\infty} \frac{1}{k^2} \sin \left(k\pi \frac{1}{x_{eD}} \right) \cos \left(k\pi \frac{x_{wD}}{x_{eD}} \right) \cos \left(k\pi \frac{x_D}{x_{eD}} \right) G(x_{eD}, y_{eD}, y_{wD}, y_D, k)
 \end{aligned} \quad (10)$$

Where the G-function is:

$$\begin{aligned}
 G(x_{eD}, y_{eD}, y_{wD}, y_D, k) &= \\
 & \frac{\cosh k\pi \left(\frac{y_{eD} - |y_D - y_{wD}|}{x_{eD}} \right) + \cosh k\pi \left(\frac{y_{eD} - (y_D + y_{wD})}{x_{eD}} \right)}{\sinh \left(k\pi \frac{y_{eD}}{x_{eD}} \right)}
 \end{aligned} \quad (11)$$

For the case of infinite conductivity fractures, the dimensionless pressure can be obtained by evaluating the above equation at $x_D = 0.732$ [14].

2.3.2. Horizontal wells

The pressure distribution equation for a horizontal well in a closed rectangular reservoir is [13]:

$$p_{Dh} = a_h = p_{Df} + F_1 \quad (12)$$

Where

$$\begin{aligned}
 F_1 &= \frac{2}{x_{eD} L_D} \sum_{n=1}^{\infty} \frac{1}{n} \cos(n\pi z_D) \cos(n\pi z_{wD}) \\
 & \times \frac{\cosh n\pi \left(\frac{y_{eD} - |y_D - y_{wD}|}{x_{eD}} \right) + \cosh n\pi \left(\frac{y_{eD} - (y_D + y_{wD})}{x_{eD}} \right)}{\sinh \left(n\pi \frac{y_{eD}}{x_{eD}} \right)} \\
 & + 4 \sum_{n=1}^{\infty} \cos(n\pi z_D) \cos(n\pi z_{wD}) \sum_{k=1}^{\infty} \frac{1}{k} \frac{\sin \left(k\pi \frac{1}{x_{eD}} \right) \cos \left(k\pi \frac{x_{wD}}{x_{eD}} \right) \cos \left(k\pi \frac{x_D}{x_{eD}} \right)}{\sqrt{b}} \\
 & \frac{\cosh \sqrt{b} (y_{eD} - |y_D - y_{wD}|) + \cosh \sqrt{b} (y_{eD} - (y_D + y_{wD}))}{\sinh(\sqrt{b} y_{eD})}
 \end{aligned} \quad (13)$$

Where $b = n^2 \pi^2 L_D^2 + k^2 \pi^2 / x_{eD}^2$ and the L term in the dimensionless definition is the horizontal well half-length $L = L_h/2$, and $z_D = z/h$ and $L_D = 1/h_D = L/2h$. x_{wD} and y_{wD} are at the mid-point of the well length for the uniform flux horizontal well case. For the infinite conductivity horizontal well case, Ozkan showed that the point $x_D = 0.732$ used to calculate pressure distribution for an infinite conductivity fracture can also be used for an infinite conductivity horizontal well [13]. The term F_1 can be rewritten as follows:

$$F_1 = \frac{2}{x_{eD} L_D} \sum_{n=1}^{\infty} \frac{1}{n} \cos(n\pi z_D) \cos(n\pi z_{wD}) G(x_{eD}, y_{eD}, y_{wD}, y_D, n\pi) + 4 \sum_{n=1}^{\infty} \cos(n\pi z_D) \cos(n\pi z_{wD}) \sum_{k=1}^{\infty} \frac{1}{k} \sin\left(k\pi \frac{1}{x_{eD}}\right) \cos\left(k\pi \frac{x_{wD}}{x_{eD}}\right) \cos\left(k\pi \frac{x_D}{x_{eD}}\right) GH\left(y_{eD}, y_{wD}, y_D, \sqrt{b}\right) \quad (14)$$

Where:

$$b = n^2 \pi^2 L_D^2 + \frac{k^2 \pi^2}{x_{eD}^2} GH(y_{eD}, y_{wD}, y_D, \sqrt{b}) = \frac{G(1, y_{eD}, y_{wD}, y_D, \sqrt{b})}{\sqrt{b}}$$

To calculate F_1 as suggested by Ozkan [13]:

$$F_1 = F + F_{b1} + F_{b2} + F_{b3} \quad (15)$$

Where

$$F = \sum_{n=1}^{\infty} \cos(n\pi z_D) \cos(n\pi z_{wD}) \int_{-1}^{+1} K_0 \left[n\pi L_D \sqrt{(x_D - x_{wD} - \alpha)^2 + (y_D - y_{wD})^2} \right] d\alpha \quad (16)$$

$$F_{b1} = \frac{2}{x_{eD} L_D} \sum_{n=1}^{\infty} \frac{1}{n} \cos(n\pi z_D) \cos(n\pi z_{wD}) \left\{ \left[e^{-n\pi L_D (y_D + y_{wD})} + e^{-n\pi L_D (2y_{eD} - |y_D - y_{wD}|)} + e^{-n\pi L_D (2y_{eD} - (y_D + y_{wD}))} \right] \left[1 + \sum_{m=1}^{\infty} e^{-2m\pi L_D y_{eD}} \right] + e^{-n\pi L_D |y_D - y_{wD}|} \sum_{m=1}^{\infty} e^{-2m\pi L_D y_{eD}} \right\} \quad (17)$$

$$F_{b2} = 4 \sum_{n=1}^{\infty} \cos(n\pi z_D) \cos(n\pi z_{wD}) \sum_{k=1}^{\infty} \frac{1}{k} \frac{\sin\left(k\pi \frac{1}{x_{eD}}\right) \cos\left(k\pi \frac{x_D}{x_{eD}}\right) \cos\left(k\pi \frac{x_{wD}}{x_{eD}}\right)}{\sqrt{n^2 \pi^2 L_D^2 + \frac{k^2 \pi^2}{x_{eD}^2}}} \quad (18)$$

$$\times \left\{ e^{-\sqrt{n^2 \pi^2 L_D^2 + \frac{k^2 \pi^2}{x_{eD}^2}} (y_D + y_{wD})} + e^{-\sqrt{n^2 \pi^2 L_D^2 + \frac{k^2 \pi^2}{x_{eD}^2}} (2y_{eD} - (y_D + y_{wD}))} + e^{-\sqrt{n^2 \pi^2 L_D^2 + \frac{k^2 \pi^2}{x_{eD}^2}} (2y_{eD} - |y_D - y_{wD}|)} \right\} \times \left[1 + \sum_{m=1}^{\infty} e^{-2m\sqrt{n^2 \pi^2 L_D^2 + \frac{k^2 \pi^2}{x_{eD}^2}} y_{eD}} \right] + e^{-\sqrt{n^2 \pi^2 L_D^2 + \frac{k^2 \pi^2}{x_{eD}^2}} |y_D - y_{wD}|} \sum_{m=1}^{\infty} e^{-2m\sqrt{n^2 \pi^2 L_D^2 + \frac{k^2 \pi^2}{x_{eD}^2}} y_{eD}} \quad (19)$$

$$F_{b3} = \sum_{n=1}^{\infty} \cos(n\pi z_D) \cos(n\pi z_{wD}) \left\{ \int_{-1}^{+1} K_0 \left[n\pi L_D \sqrt{(x_D + x_{wD} - \alpha)^2 + (y_D - y_{wD})^2} \right] d\alpha + \sum_{k=1}^{\infty} \int_{-1}^{+1} \left\{ K_0 \left[n\pi L_D \sqrt{(x_D - x_{wD} - 2kx_{eD} - \alpha)^2 + (y_D - y_{wD})^2} \right] + K_0 \left[n\pi L_D \sqrt{(x_D + x_{wD} - 2kx_{eD} - \alpha)^2 + (y_D - y_{wD})^2} \right] + K_0 \left[n\pi L_D \sqrt{(x_D - x_{wD} + 2kx_{eD} - \alpha)^2 + (y_D - y_{wD})^2} \right] + K_0 \left[n\pi L_D \sqrt{(x_D + x_{wD} + 2kx_{eD} - \alpha)^2 + (y_D - y_{wD})^2} \right] \right\} d\alpha \right\} \quad (19)$$

For the case of $y_D = y_{wD}$ if $|X| \leq a$ then

$$\int_{-a}^{+a} K_0 \left[b\sqrt{(X - \alpha)^2} \right] d\alpha = \frac{1}{b} \left[\int_0^{b(a+X)} K_0(u) du + \int_0^{b(a-X)} K_0(u) du \right] \quad (20)$$

If $|X| \geq a$ then

$$\int_{-a}^{+a} K_0 \left[b\sqrt{(X - \alpha)^2} \right] d\alpha = \frac{1}{b} \left[\int_0^{b(|X|+a)} K_0(u) du - \int_0^{b(|X|-a)} K_0(u) du \right] \quad (21)$$

If $|X| = a$ then

$$\int_{-a}^{+a} K_0 \left[b\sqrt{(X - \alpha)^2} \right] d\alpha = \frac{1}{b} \int_0^{2ab} K_0(u) du \quad (22)$$

Where $a = 1, b = n\pi L_D$

Table 1 presents the dimensionless coordinates for all the vertically fractured wells in the 5×4 synthetic field (5 injectors: I1, I2, I3, I4 and I5 and 4 producers: P1, P2, P3 and P4 as shown on Figure 1). All wells have the same fracture half-length of 145 ft. Other data include $x_{eD} = y_{eD} = 21.38$ and $r_{wD} = 0.0049$. Table 2 shows the shape factors for all the wells in the 5×4 synthetic field calculated using P_{wD} results (influence functions) from the different calculation techniques and Equation 9. As shown in Table 2, the shape factors are in good agreement. These shape factors can be used to calculate the influence functions using Equation 8.

Table 3 presents the dimensionless coordinates for all the wells in the 5×4 homogeneous synthetic field. Other data include $x_{eD} = y_{eD} = 20.67$ and $r_{wD} = 0.004733$. Table 4 shows the shape factors for the horizontal wells in the 5×4 synthetic field calculated using P_{wD} results (influence functions) from Equations 9 and 12.

Table 1. Dimensionless coordinates of the fractured wells in the 5×4 synthetic field

Wells	x_{wDf}	y_{wDf}
I01	3.7931	17.5862
I02	17.5862	17.5862
I03	10.6897	10.6897
I04	3.7931	3.7931
I05	17.5862	3.7931
P01	10.6897	17.5862
P02	3.7931	10.6897
P03	17.5862	10.6897
P04	10.6897	3.7931

Table 2. Shape factors for the fractured wells in the 5 × 4 synthetic field calculated for different fracture types

Wells	C _{Af}	
	Uniform Flux	Infinite Conductivity
I01	0.1144	0.2665
I02	0.1140	0.1606
I03	4.1698	7.5580
I04	0.1144	0.2665
I05	0.1140	0.1606
P01	0.9083	1.6560
P02	0.9026	1.9678
P03	0.9003	1.3396
P04	0.9083	1.6560

Table 3. Dimensionless coordinates of the horizontal wells in the 5 × 4 synthetic field

Wells	x _{wDh}	y _{wDh}
I01	3.6667	17.0000
I02	17.0000	17.0000
I03	10.3333	10.3333
I04	3.6667	3.6667
I05	17.0000	3.6667
P01	10.3333	17.0000
P02	3.6667	10.3333
P03	17.0000	10.3333
P04	10.3333	3.6667

Table 4. Shape factors for uniform flux and infinite conductivity horizontal wells in 5 × 4 synthetic reservoir

Wells	C _{Ah}	
	Uniform Flux	Infinite Conductivity
I01	0.0404	0.0950
I02	0.0403	0.0563
I03	1.4741	2.6713
I04	0.0404	0.0950
I05	0.0403	0.0563
P01	0.3212	0.5857
P02	0.3190	0.6997
P03	0.3182	0.4699
P04	0.3212	0.5857

3. Simulation results for hydraulically fractured wells

3.1. Model descriptions for hydraulically fractured wells

The grids in the small areas containing the wells were refined using the Local Grid Refinement (LGR) options. Thus, there are nine LGRs in this model [15]. Figure 1 shows the top view of the permeability distribution for this case. The LGRs can be seen at each well. Figure 2 is a permeability distribution plot showing the cross-sectional view through three wells. The hydraulic fractures are represented in red indicating high permeability. The LGR areas are 300 ft × 20 ft each with a global grid configuration of 13 × 1 which is refined to a grid configuration of 65 × 25.

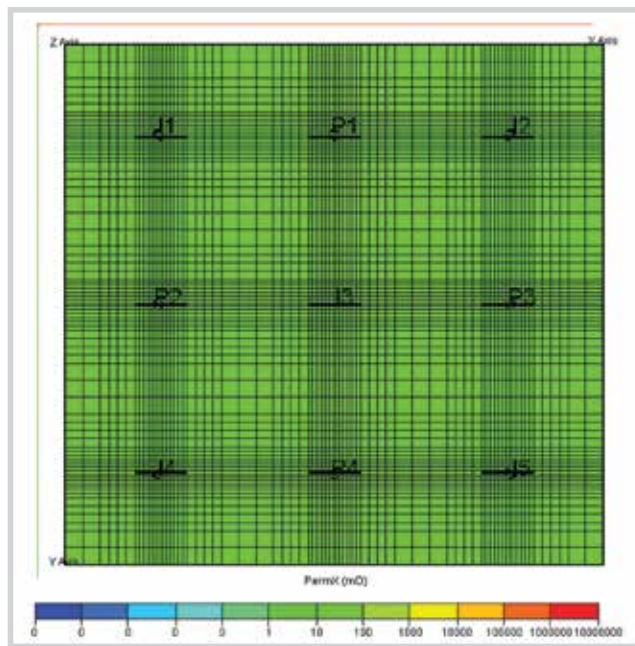


Figure 1. Top view of the simulation model showing the LGRs at the fractured wells in the 5 × 4 homogeneous synthetic field.

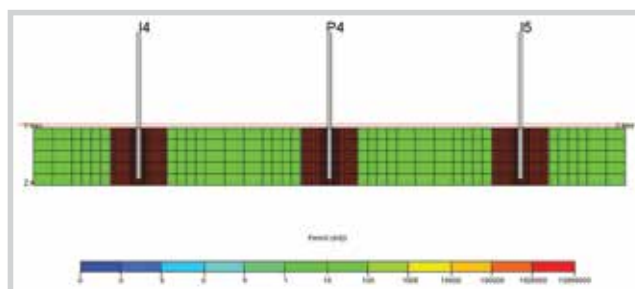


Figure 2. Cross sectional view showing three wells and the hydraulic fractures in the 5 × 4 homogeneous synthetic reservoir.

No refinement in the vertical direction was applied. Thus, the number of layers in the LGRs stayed at five layers.

Figure 3 presents a zoom-in top view of a LGR containing a high permeability strip representing a hydraulic fracture. Notice that the permeability of the cell at the tips of the fracture was set to zero following the assumption that there was no flow through the tips of the fracture. The permeability of the fractures was set to 8,000 Darcys. The width of the fractures was 0.8 ft, and the fracture half-lengths were the same at 145 ft. Thus, the dimensionless fracture conductivity for every fracture, which is the product of fracture permeability and fracture width divided by the product of formation permeability and fracture half-length, is equal to 441. Thus, according to previous studies [16, 17], the fractures can be considered as infinite conductivity fractures (dimensionless fracture conductivity is larger than 300). The porosity of the fracture was input as 0.6 which is higher than the porosity of the formation of 0.3.

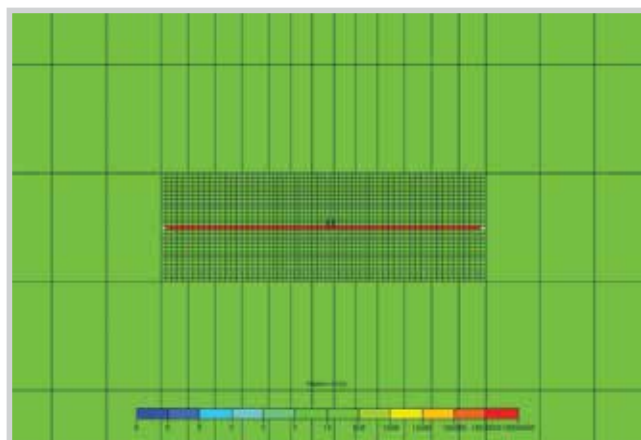


Figure 3. A zoom-in view of a LGR showing a high permeability strip representing a hydraulic fracture - 5×4 homogeneous system.

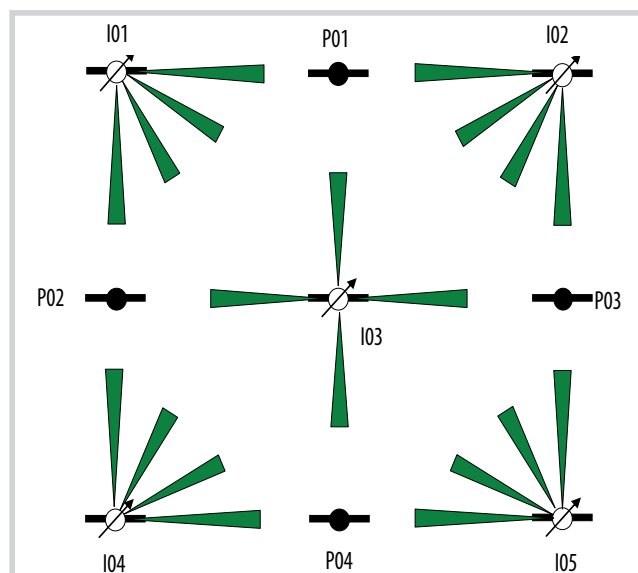


Figure 5. Representation of the relative interwell permeability for the 5×4 homogeneous reservoir with hydraulically fractured wells.

3.2. Homogeneous reservoir with hydraulic fractures

Table 5 and Figure 4 show the results for the interwell connectivity coefficients. Similar to previous cases, the results are as good as the results obtained in the case of homogeneous reservoir with vertical wells only with asymmetry coefficient of 0.0048. Table 6 and Figure 5 present the corresponding relative interwell permeabilities with the equivalent time of 5.66 days, and the reference permeability of 100 mD. The difference between the high and low interwell connectivity coefficients is more significant than in the case of vertical wells suggesting an observation well is less affected by a far away active fractured well than by a vertical unfractured well of the same distance away. This is reasonable because with the same flow rate, the pressure drop in a fractured well is less than its unfractured counterpart.

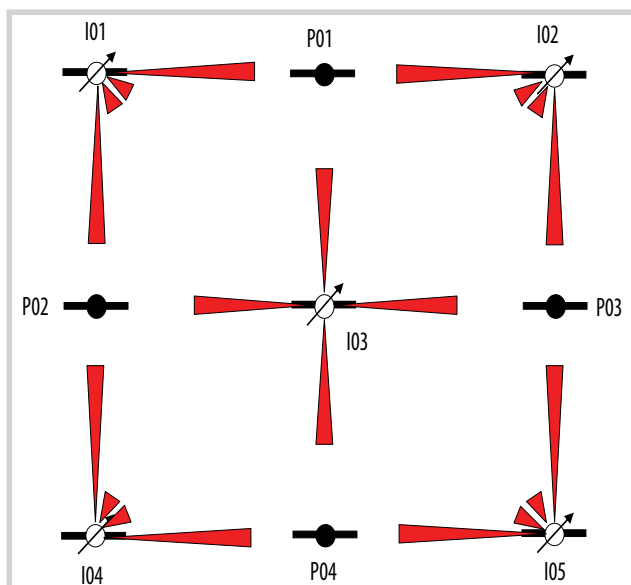


Figure 4. Representation of the interwell connectivity coefficients for the 5×4 homogeneous system with hydraulically fractured wells.

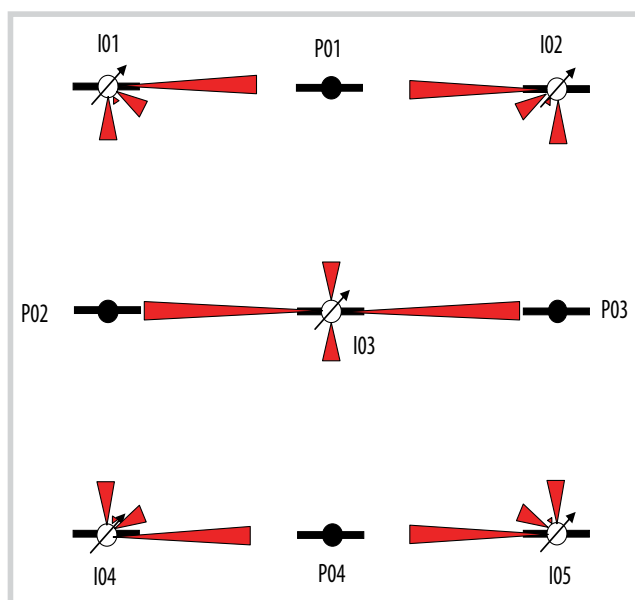


Figure 6. Representation of the connectivity coefficients for the case of 5×4 anisotropic reservoir - hydraulically fractured wells.

3.3. Anisotropic reservoir with hydraulic fractures

Similar to the anisotropic case in the previous chapter, the effective permeability in the x direction is tenfold the fracture permeability in the y direction. Table 7 and Figure 6 show the results for the interwell connectivity coefficients. As expected, the results are good indications of the anisotropy with large coefficients for well pairs in the direction of high permeability. Table 8 and Figure 7 present the corresponding relative interwell permeabilities with the equivalent time of 5.66 days, and the reference permeability of 316 mD.

Table 5. Interwell connectivity coefficient results from simulation data for the 5 × 4 homogeneous synthetic field with hydraulic fractured wells ($A_f = 0.0048$)

	P1	P2	P3	P4	Sum
β_{0j} (psia)	-223.6	-226.1	-225.7	-223.6	-899
I1	0.32	0.31	0.06	0.06	0.75
I2	0.32	0.06	0.31	0.06	0.75
I3	0.24	0.25	0.26	0.25	1.01
I4	0.06	0.31	0.06	0.32	0.75
I5	0.06	0.06	0.31	0.32	0.75
Sum	1.00	1.00	1.00	1.00	

Table 7. Interwell connectivity coefficient results from simulation data for the 5 × 4 anisotropic synthetic field - hydraulically fractured wells

	P1	P2	P3	P4	Sum
β_{0j} (psia)	-69.6	-96.5	-96.5	-69.6	-332
I1	0.43	0.13	0.10	0.02	0.67
I2	0.43	0.10	0.13	0.02	0.67
I3	0.11	0.55	0.55	0.11	1.32
I4	0.02	0.13	0.10	0.42	0.67
I5	0.02	0.10	0.13	0.43	0.67
Sum	1.00	1.00	1.00	1.00	

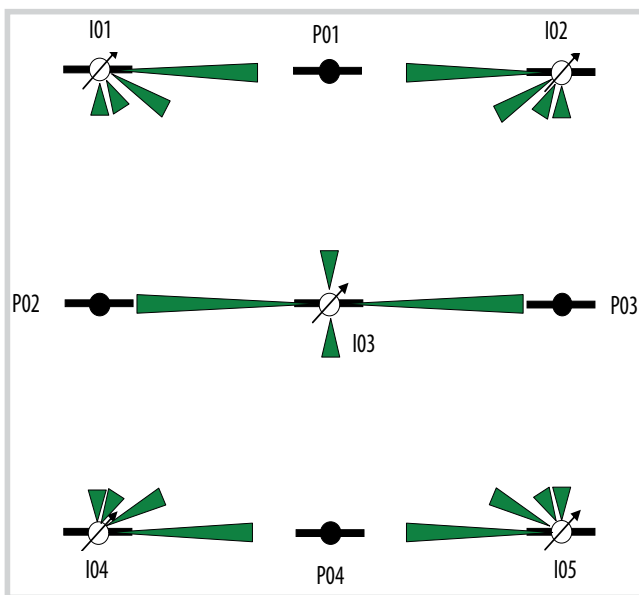


Figure 7. Representation of relative interwell permeability for the case of 5 × 4 synthetic reservoir - hydraulically fractured wells.

3.4. Reservoir with a high permeability channel

Figure 8 shows the top view of the permeability distribution for this case. The cells in yellow color have high permeability in both x and y direction. Similar to the high permeability channel cases in the previous chapters, the permeability of the channel was ten-fold (1,000 mD) of that in the other areas of the reservoir (100 mD). There are nine vertically fractured wells with the same fracture half-length of 145 ft.

Table 6. Relative interwell permeability results for the 5 × 4 homogeneous synthetic field with hydraulic fractured wells ($k_{ref} = 100$ mD, $\Delta t_{eq} = 5.66$ days)

	P1	P2	P3	P4	Average
I1	114	112	90	91	102
I2	114	91	111	91	102
I3	92	96	99	93	95
I4	92	111	91	114	102
I5	91	92	113	117	103
Average	101	101	101	101	

Table 8. Relative interwell permeability results for the 5 × 4 anisotropic synthetic field - hydraulically fractured wells ($k_{ref} = 316$ mD, $\Delta t_{eq} = 5.66$ days)

	P1	P2	P3	P4	Average
I1	353	75	152	78	164
I2	351	152	76	80	164
I3	90	444	444	90	267
I4	80	75	151	350	164
I5	77	153	77	357	166
Average	190	180	180	191	

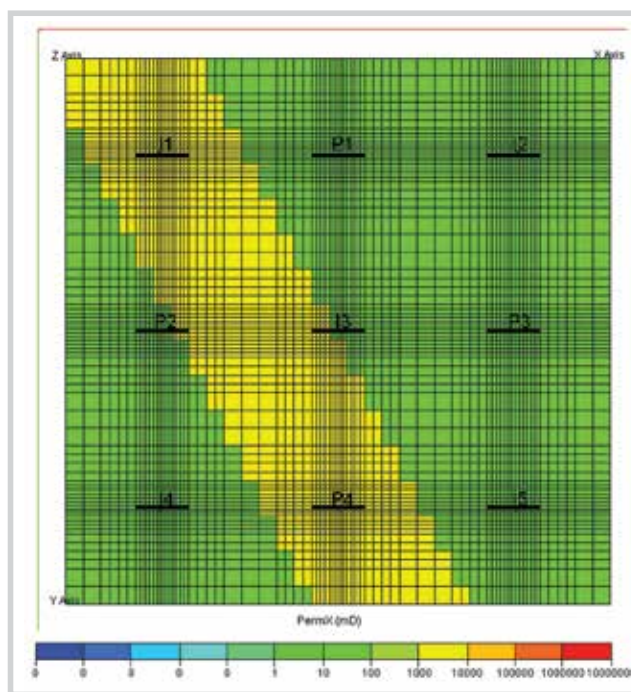


Figure 8. Top view of the simulation model showing the permeability in x direction for the high permeability channel case of the 5 × 4 synthetic field with fractured wells.

Table 9 and Figure 9 show the results for the interwell connectivity coefficients. Similar to previous cases of high permeability channels, the results reflect well the presence of the channel. Different from the previous cases, well I03 has much higher connectivity with producers P02 and P04. The reason for this is that in the previous cases, well I03 was not connected to the high permeability channel while in this case, due to the extension provided by the hydraulic fracture, it is directly connected to the channel and has better connectivity with the producers.

Table 9. Interwell connectivity coefficient results from simulation data for the 5 × 4 synthetic reservoir with a high permeability channel - hydraulically fractured wells

	P1	P2	P3	P4	Sum
β_{0j} (psia)	-153.5	-54.1	-194.2	-65.4	-467
I1	0.46	0.42	0.10	0.16	1.14
I2	0.23	0.02	0.28	0.02	0.55
I3	0.26	0.45	0.33	0.53	1.57
I4	0.02	0.07	0.03	0.13	0.25
I5	0.03	0.04	0.25	0.16	0.48
Sum	1.00	1.00	1.00	1.00	

Table 10. Relative interwell permeability results for the 5 × 4 synthetic reservoir with high permeability channel - hydraulically fractured wells. ($k_{ref} = 300$ mD, $\Delta t_{eq} = 5.66$ days)

	P1	P2	P3	P4	Average
I1	369	337	153	200	265
I2	162	77	210	84	133
I3	202	347	256	412	304
I4	79	24	92	69	66
I5	90	94	184	104	118
Average	180	176	179	174	

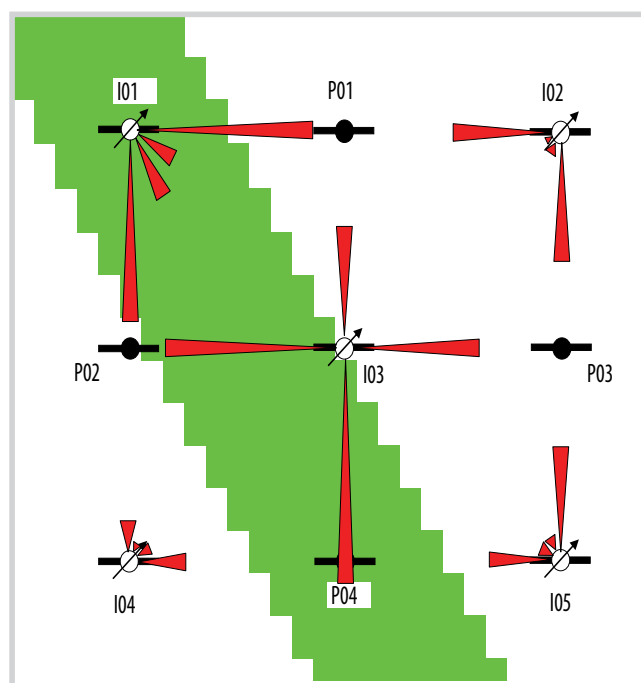


Figure 9. Representation of the connectivity coefficients for the case of 5 × 4 synthetic reservoir with a high permeability channel - hydraulically fractured wells.

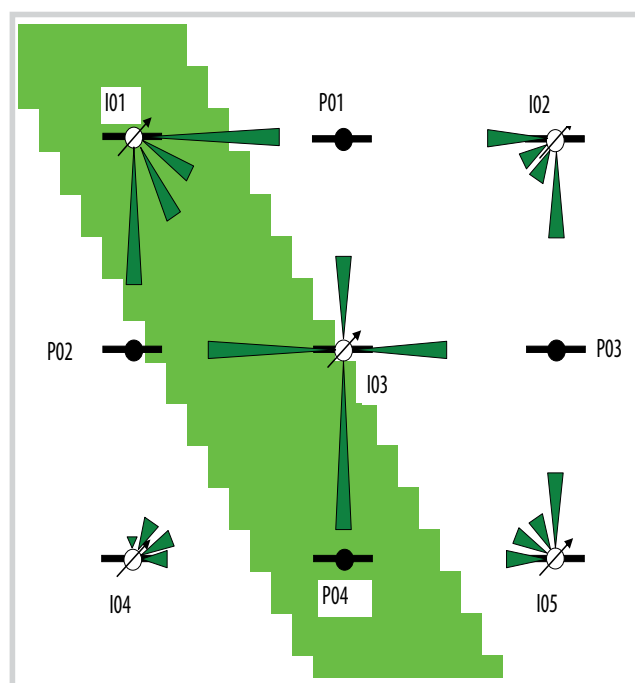


Figure 10. Representation of relative interwell permeability for the 5 × 4 synthetic reservoir with a high permeability channel - hydraulically fractured wells.

Table 10 and Figure 10 present the corresponding relative interwell permeabilities with the equivalent time of 5.66 days, and the reference permeability of 300 mD.

3.5. Reservoir with a partially sealing barrier

Figure 11 shows the top view of the x-direction permeability distribution for this case. The permeability for the cells in grey color were set to zero and thus, those cells served as a partially sealing barrier. The formation permeability was 100 mD.

Table 11 and Figure 12 show the results for the interwell connectivity coefficients. The presence of the partially sealing barrier is well established by the results. Table 12 and Figure 13 present the corresponding relative interwell permeabilities with the equivalent time of 5.66 days, and the reference permeability of 100 mD. The relative interwell permeability for well pair I01-P01 was negative because the influence function for the pair was calculated using the late time solution. When the interwell connectivity coefficients are small, they are translated to early

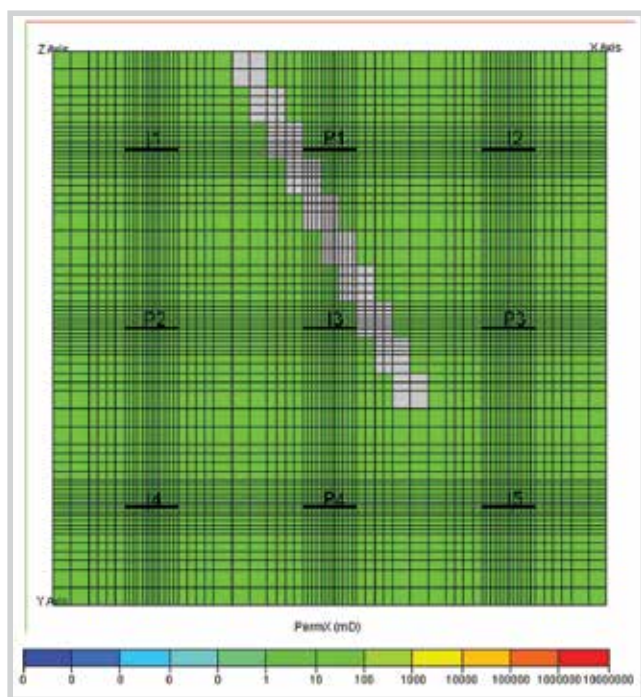


Figure 11. Top view of the simulation model showing the permeability distribution in x direction for the case of 5 × 4 synthetic field with a partially sealing barrier - hydraulically fractured wells.

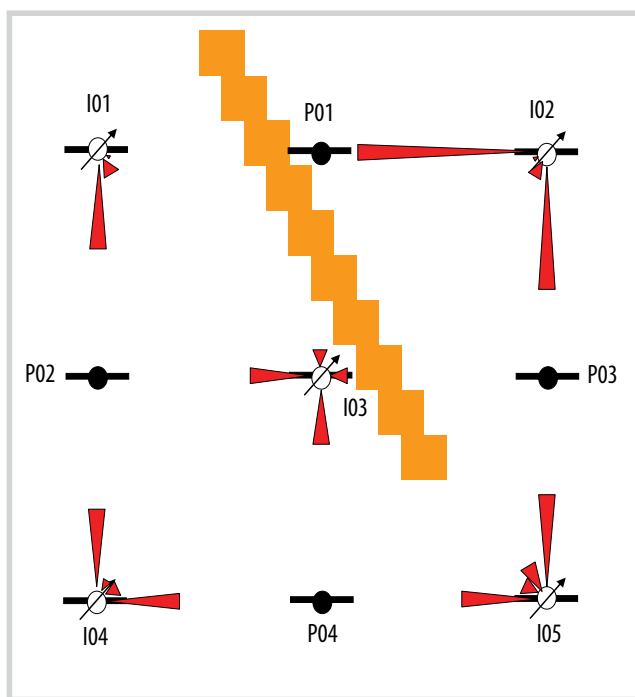


Figure 12. Representation of the connectivity coefficients for the case of 5 × 4 dual-porosity reservoir with a partially sealing barrier - hydraulically fractured wells.

Table 11. Interwell connectivity coefficient results from simulation data for the 5 × 4 synthetic field with partially sealing barrier - hydraulically fractured wells

	P1	P2	P3	P4	Sum
β_{oj} (psia)	-440.1	-204.0	-306.9	-226.1	-1177
I1	0.01	0.34	0.01	0.06	0.42
I2	0.79	0.02	0.49	0.06	1.36
I3	0.06	0.25	0.08	0.22	0.61
I4	0.04	0.32	0.05	0.33	0.73
I5	0.11	0.07	0.37	0.33	0.87
Sum	1.00	1.00	1.00	1.00	

Table 12. Relative interwell permeability results for the 5 × 4 synthetic field with partially sealing barrier - hydraulically fractured wells ($k_{rel} = 100$ mD, $\Delta t_{eq} = 5.66$ days)

	P1	P2	P3	P4	Average
I1	-40	127	68	90	62
I2	347	71	199	92	177
I3	23	95	29	83	58
I4	80	114	88	119	100
I5	115	95	141	125	119
Average	105	101	105	102	

time periods and thus the late time solution becomes inaccurate. Solutions that are good for both early time and late time should be used for better results.

3.6. Reservoir with a sealing barrier

Figure 14 shows the top view of the x-direction permeability distribution with a sealing barrier case. The permeability of the cells in grey color was set to zero and thus, those cells served as a sealing barrier. As seen in the figure, the barrier completely divides the reservoir into

two compartments. Based on the change in average reservoir pressure calculated from each producer, this compartmentalisation can be inferred.

Table 13 and Figure 15 show the results for the interwell connectivity coefficients. Similar to previous cases, the results clearly reflect the presence of the sealing barrier. Some connectivity coefficients are very small and even negative. They indicate poor connectivity or no connectivity at all. Small connectivities were still observed for some pairs of wells on different sides of the sealing barrier.

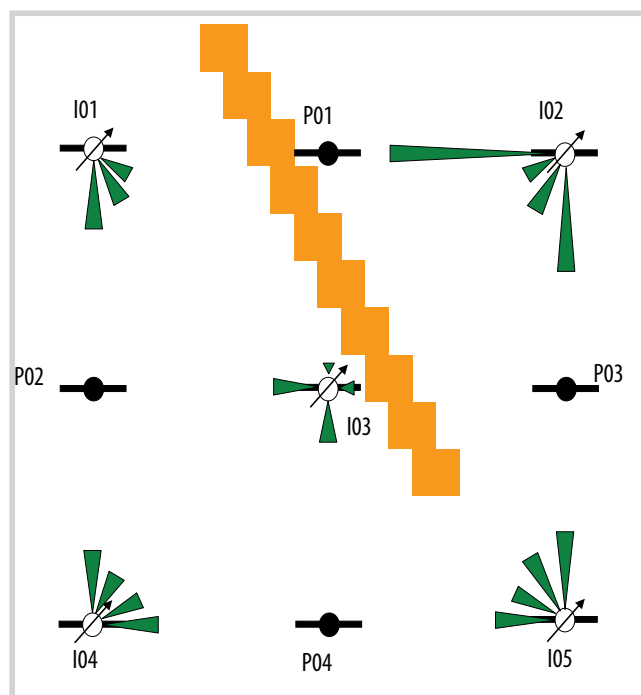


Figure 13. Representation of relative interwell permeability for the case of 5 × 4 dual-porosity reservoir with a partially sealing barrier - hydraulically fractured wells.

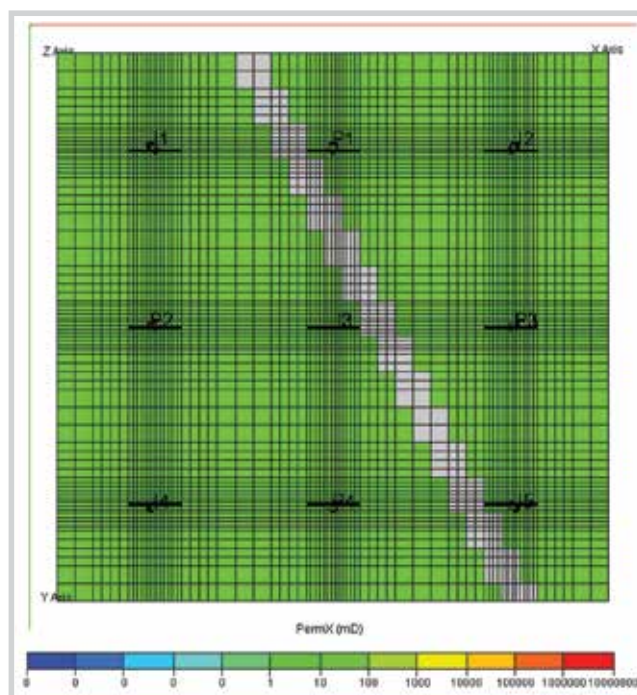


Figure 14. Top view of the simulation model showing the permeability in x direction for the case of 5 × 4 synthetic field with a sealing barrier - hydraulically fractured wells.

Table 13. Interwell connectivity coefficient results from simulation data for the 5 × 4 synthetic field with a sealing barrier - hydraulically fractured wells

	P1	P2	P3	P4	Sum
β_{oj} (psia)	-336.6	-266.0	-225.4	-365.7	-1194
I1	0.00	0.35	0.00	0.10	0.45
I2	0.87	-0.01	0.60	-0.01	1.44
I3	0.05	0.27	0.05	0.35	0.73
I4	-0.02	0.36	-0.02	0.53	0.84
I5	0.07	0.04	0.35	0.05	0.51
Sum	0.97	1.01	0.97	1.02	

Table 14. Relative interwell permeability results for the 5 × 4 synthetic field with a sealing barrier - hydraulically fractured wells ($k_{ref} = 100$ mD, $\Delta t_{eq} = 5.66$ days)

	P1	P2	P3	P4	Average
I1	0.00	131.5	0.00	112.5	61.01
I2	385.6	0.00	253.1	0.00	159.7
I3	0.00	101.7	0.00	132.6	58.6
I4	0.00	137.4	0.00	216.6	88.5
I5	98.2	0.00	132.6	0.00	57.7
Average	97	74	77	92	

As explained before, these non-zero connectivity coefficients are due to the noises in the data as the injection rates were generated randomly. This problem can be resolved by increasing the number of data points. For this case, the interwell connectivity coefficients should be analysed with the average reservoir pressure change results. If the pressure changes indicate reservoir compartmentalisation, then the small interwell connectivity coefficients can be evaluated to decide whether the injectors and producers are on different side of the barrier.

Table 14 and Figure 16 present the corresponding relative interwell permeabilities with the equivalent time of 5.66 days, and the reference permeability of 100 mD. A cut-off coefficient of 0.06 was applied to eliminate the low connectivity coefficients. Thus, the relative interwell permeability corresponding to the coefficients lower than 0.06 were set to zeros. The resulting relative interwell permeabilities show a clear presence of the sealing barrier.

Table 15 shows the results for the average reservoir pressure change for all producers in each case described

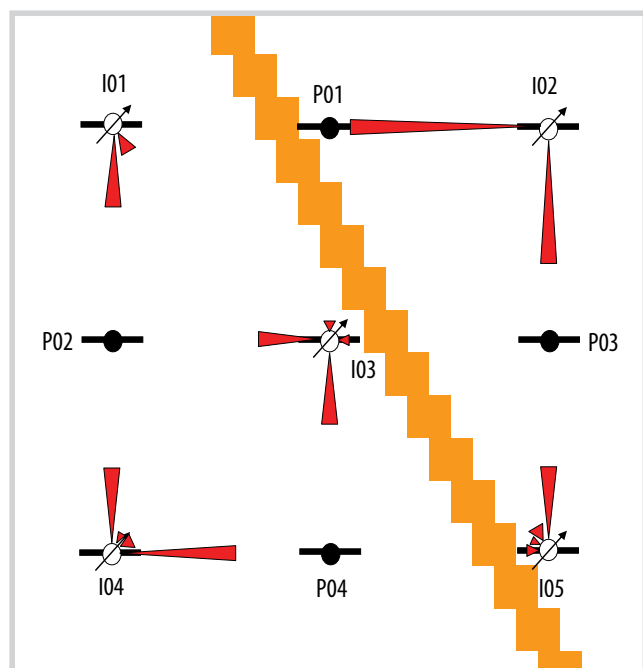


Figure 15. Representation of the connectivity coefficients for the 5 × 4 synthetic field with a sealing barrier - hydraulically fractured wells.

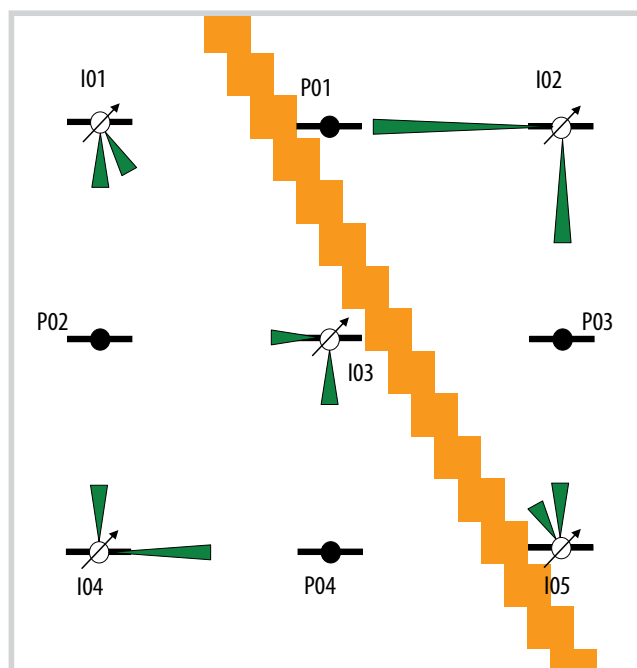


Figure 16. Representation of relative interwell permeability for the 5 × 4 synthetic field with a sealing barrier - hydraulically fractured wells.

Table 15. Average pressure change (ΔP_{ave}) after each time interval for different cases of 5 × 4 synthetic field - hydraulically fractured wells

Cases	P1	P2	P3	P4
Homogeneous eservoir	285.93	285.93	285.74	285.74
Anisotropic reservoir	285.83	285.82	285.82	285.77
Channel	285.82	285.82	285.81	285.82
Partially sealing barrier	295.33	300.01	296.38	298.84
Sealing barrier	180.93	390.14	180.77	390.18

above. Similar to the results obtained from the previous systems, except for the case of sealing barrier, the changes in average reservoir pressure for all the cases are consistent and close to the pressure changes obtained from the simulation results. For the case with the presence of sealing barrier, the calculated pressure changes for wells P01 and P03 (about 181 psi) are different from those for wells P02 and P04 (about 390 psi) indicating two different pore volumes and thus, two different reservoir compartments.

4. Simulation results for horizontal wells

4.1. Model description for horizontal wells

Figure 17 shows the top view of the permeability distribution of the 5 × 4 homogeneous synthetic field with horizontal wells. All the wells were horizontal wells with their centres at the cell where the vertical wells were completed as described in the previous section (Table 3). Figure 18 shows the permeability distribution cross section cutting through three representative horizontal wells. Thus, all the wells were completed in the centre

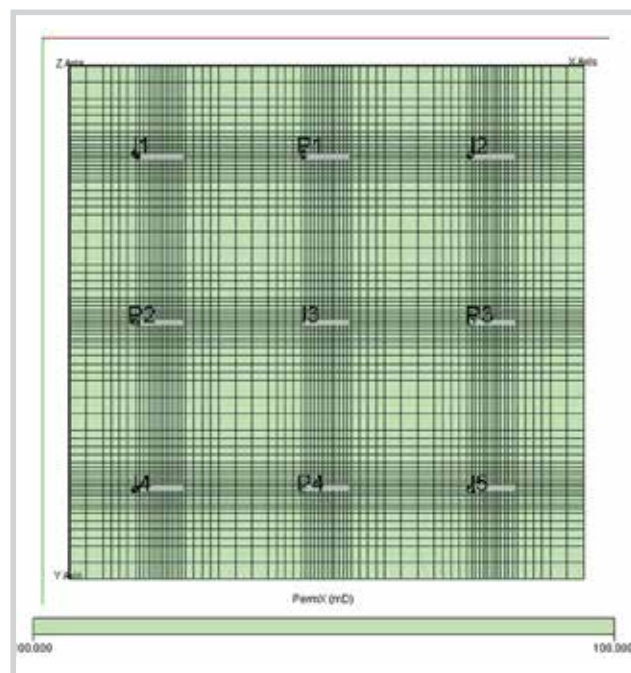


Figure 17. Top view of the simulation model showing the horizontal wells of the 5 × 4 homogeneous synthetic field.

layer of the reservoir so that their distances to the top and bottom boundaries of the reservoir were equal. The formation permeability was set to 100 mD in the x, y and z directions. All wells are at the same length of 300 ft and completed along the x-direction. The wells were assumed to be infinite conductivity horizontal wells. Thus, the influence functions were calculated using the pressure distribution equation (Equation 12) evaluated at the point $x_D = 0.732$ and $y_D = y_{wD}$.

4.2. Homogeneous reservoir

Table 16 and Figure 19 show the results for the interwell connectivity coefficients obtained from the simulation data for this case. Similar to the same cases in the previous section, the results are very close to the results obtained for the homogeneous reservoir with vertical wells. Small value of the asymmetry coefficient for this case ($A_s = 0.00445$) indicates good results for the interwell connectivity coefficients. Table 17 and Figure 20 present the corresponding relative interwell permeabilities with the equivalent time of 6.59 days, and the reference per-

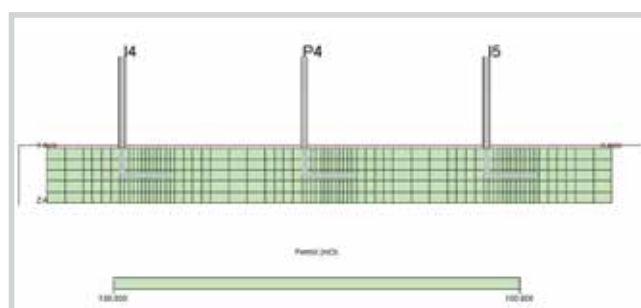


Figure 18. Cross sectional view showing three horizontal wells and their completions in the 5 × 4 homogeneous synthetic reservoir.

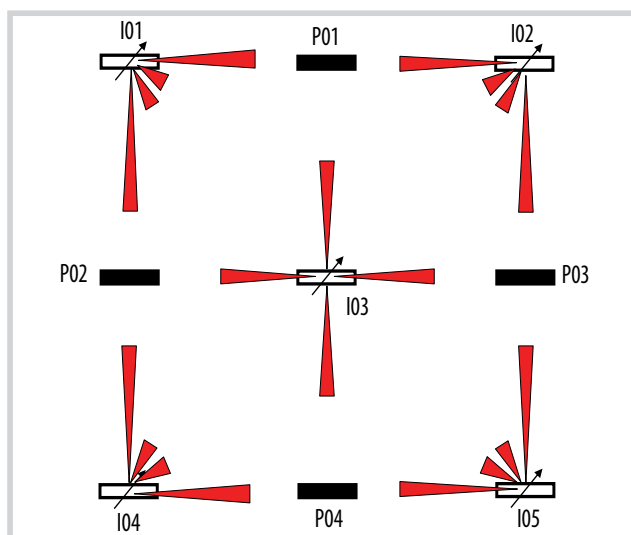


Figure 19. Representation of the connectivity coefficients for the case of 5 × 4 homogeneous reservoir with horizontal wells.

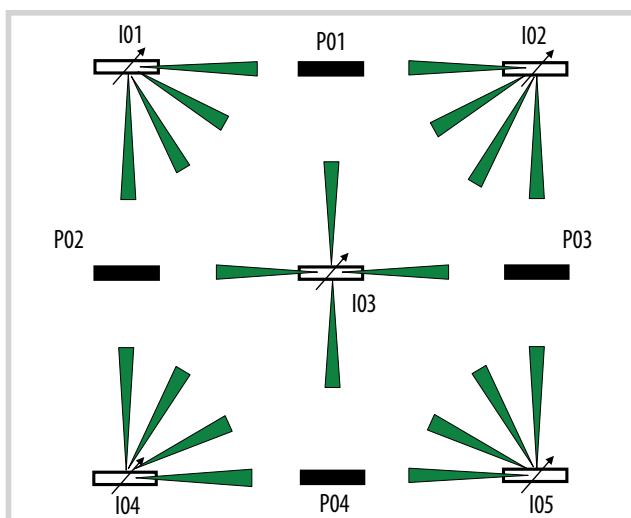


Figure 20. Representation of the relative interwell permeability for the case of 5 × 4 homogeneous reservoir with horizontal wells.

Table 16. Interwell connectivity coefficient results from simulation data for the 5 × 4 homogeneous synthetic field with horizontal wells ($A = 0.00445$)

	P1	P2	P3	P4	Sum
β_{0j} (psia)	-291.9	-293.7	-294.0	-292.1	-1172
I1	0.29	0.30	0.08	0.09	0.76
I2	0.29	0.08	0.30	0.09	0.76
I3	0.24	0.24	0.25	0.23	0.96
I4	0.09	0.29	0.09	0.29	0.76
I5	0.09	0.09	0.29	0.30	0.76
Sum	1.00	1.00	1.00	1.00	

Table 17. Relative interwell permeability results for the 5 × 4 homogeneous synthetic field with horizontal wells ($k_{ref} = 100$ mD, $\Delta t_{eq} = 6.59$ days)

	P1	P2	P3	P4	Average
I1	108	112	92	97	102
I2	107	94	109	97	102
I3	93	93	98	93	94
I4	98	107	96	106	102
I5	96	97	106	109	102
Average	100	101	100	100	

Table 18. Interwell connectivity coefficient results from simulation data for the 5 × 4 anisotropic synthetic field - horizontal wells

	P1	P2	P3	P4	Sum
β_{0j} (psia)	-131.3	-165.7	-165.7	-131.5	-594
I1	0.38	0.15	0.13	0.05	0.71
I2	0.38	0.13	0.15	0.05	0.72
I3	0.14	0.43	0.43	0.14	1.14
I4	0.05	0.15	0.13	0.38	0.71
I5	0.04	0.13	0.15	0.39	0.72
Sum	1.00	1.00	1.00	1.00	

Table 19. Relative interwell permeability results for the 5 × 4 anisotropic synthetic field - horizontal wells ($k_{ref} = 316$ mD, $\Delta t_{eq} = 6.59$ days)

	P1	P2	P3	P4	Average
I1	319	104	175	95	173
I2	317	177	105	96	174
I3	117	354	355	117	236
I4	100	103	174	314	173
I5	91	177	105	321	174
Average	189	183	183	189	

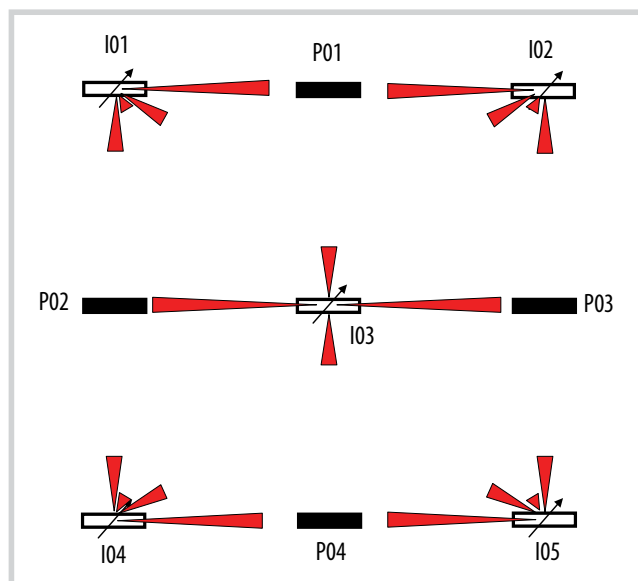


Figure 21. Representation of the interwell connectivity coefficients for the case of 5 × 4 anisotropic reservoir - horizontal wells.

meability of 100 mD. Notice that the differences between the high and low interwell connectivity coefficients are less significant than in the case of vertically fractured wells of similar half-length suggesting the observation wells are less affected by the nearby active horizontal wells than as in the vertically fractured well case. This is reasonable because for the same flow rate, the pressure drop in a fractured well is less than in a horizontal well considering the fracture half-length is approximately equal to the horizontal well half-length.

4.3. Anisotropic reservoir with horizontal wells

In this case, the effective permeability in the x-direction (1,000 mD) is tenfold the permeability in the y-direc-

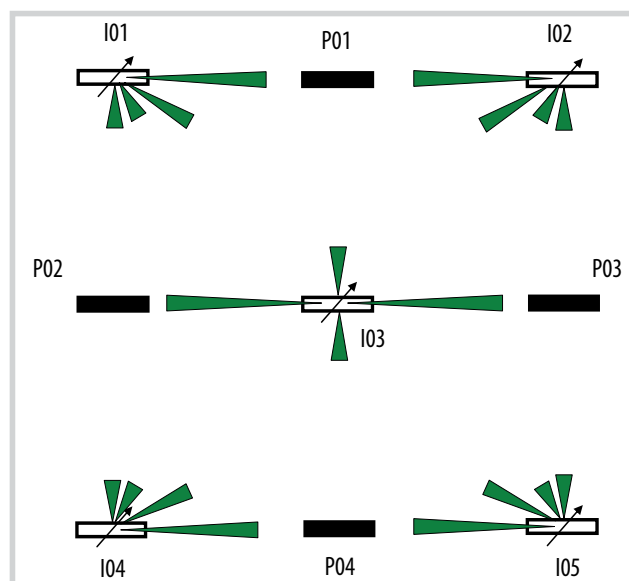


Figure 22. Representation of relative interwell permeability for the case of 5 × 4 synthetic reservoir - horizontal wells.

tion (100 mD). Similar to the homogeneous base case, all wells have the same horizontal half-lengths. Table 18 and Figure 21 show the results for the interwell connectivity coefficients. As expected, the results are good indications of the reservoir anisotropy with large coefficients for well pairs in the direction of high permeability. Table 19 and Figure 22 present the corresponding relative interwell permeabilities with the equivalent time of 6.59 days, and the reference permeability of 316 mD.

4.4. Reservoir with high permeability channel

Figure 23 shows the top view of the permeability distribution for this case. The cells in red color indicate high permeability in both x and y directions. Similar to the high

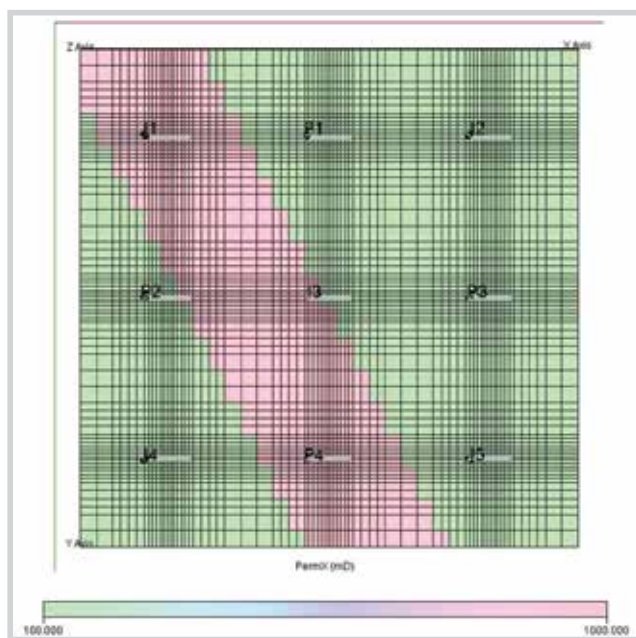


Figure 23. Top view of the simulation model showing the permeability in x-direction for the high permeability channel case of the 5 × 4 synthetic field - horizontal wells.

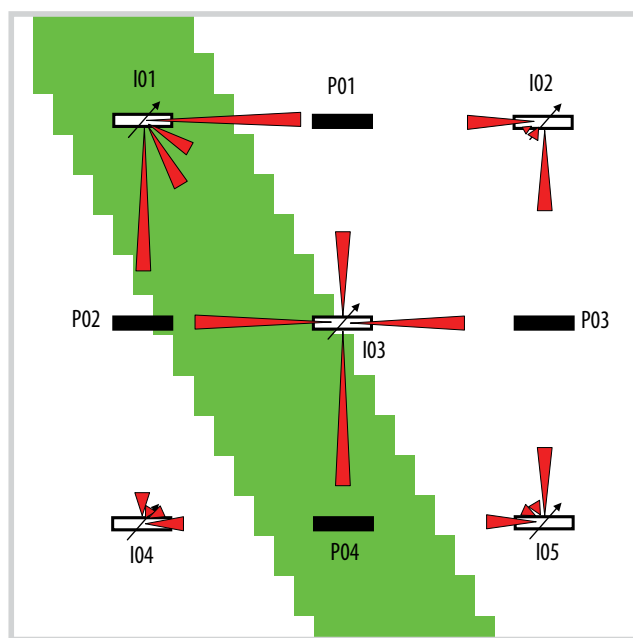


Figure 24. Representation of the connectivity coefficients for the high permeability channel case of the 5 × 4 synthetic field - horizontal wells.

Table 20. Interwell connectivity coefficient results from simulation data for the high permeability channel case of the 5 × 4 synthetic field - horizontal wells

	P1	P2	P3	P4	Sum
β_{0j} (psia)	-197.5	-73.2	-241.7	-83.5	-596
I1	0.46	0.45	0.14	0.22	1.27
I2	0.20	0.03	0.25	0.04	0.51
I3	0.26	0.41	0.34	0.48	1.50
I4	0.03	0.07	0.05	0.12	0.27
I5	0.04	0.04	0.21	0.15	0.45
Sum	1.00	1.00	1.00	1.00	

Table 21. Relative interwell permeability results for the high permeability channel case of the 5 × 4 synthetic field - horizontal wells ($k_{ref} = 300$ mD, $\Delta t_{eq} = 6.59$ days)

	P1	P2	P3	P4	Average
I1	374	368	179	245	292
I2	142	76	188	86	123
I3	209	321	271	384	296
I4	83	29	97	66	69
I5	91	92	155	95	108
Average	180	177	178	175	

permeability channel cases in the previous chapters, the permeability of the channel was ten-fold (1,000 mD) of that in the other areas of the reservoir (100 mD). There are nine horizontal wells with the same horizontal well half-length of 150 ft.

Table 20 and Figure 24 show the results for the interwell connectivity coefficients. Similar to the fractured well case of a reservoir with high permeability channel, the results reflect accurately the presence of the channel. Table 21 and Figure 25 present the corresponding relative interwell permeabilities with the equivalent time of 6.59 days, and the reference permeability of 300 mD.

4.5. Reservoir with a partially sealing barrier

Figure 26 shows the top view of the x-direction permeability distribution for this case. The cells in white color were inactive and thus, served as a partially sealing barrier. The formation permeability was 100 mD. Table 22 and Figure 26 show the results for the interwell connectivity coefficients. The presence of the partially sealing barrier is well established based on the results. Table 23 and Figure 28 present the corresponding relative interwell permeabilities with the equivalent time of 6.59 days, and the reference permeability of 100 mD. Similar to the same case for fractured wells, the relative interwell permeability

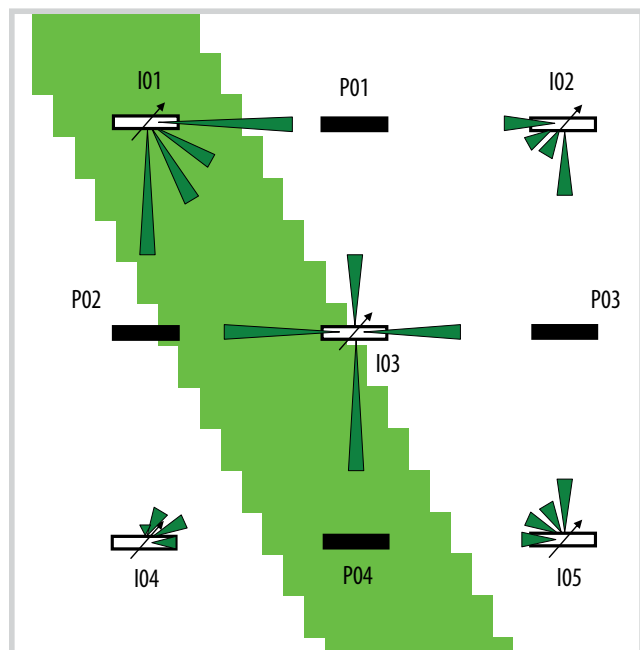


Figure 25. Representation of relative interwell permeability for the high permeability channel case of the 5 x 4 synthetic field - horizontal wells.

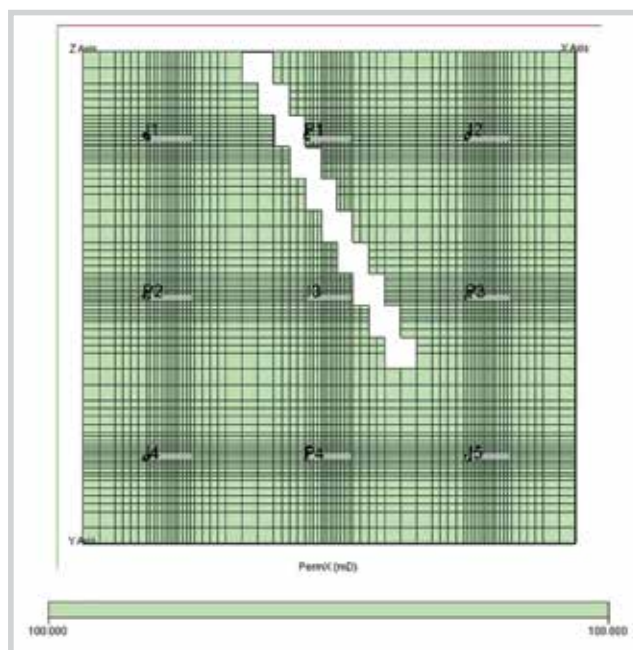


Figure 26. Top view of the simulation model showing the permeability distribution in x direction for the 5 x 4 synthetic field with partially sealing barrier - horizontal wells.

Table 22. Interwell connectivity coefficient results from simulation data for the 5 x 4 synthetic field with partially sealing barrier - horizontal wells

	P1	P2	P3	P4	Sum
β_{0j} (psia)	-540.6	-260.1	-391.4	-291.3	-1483
I1	0.01	0.34	0.02	0.09	0.46
I2	0.73	0.03	0.47	0.09	1.31
I3	0.07	0.24	0.10	0.22	0.63
I4	0.05	0.30	0.07	0.30	0.73
I5	0.13	0.09	0.34	0.31	0.87
Sum	1.00	1.00	1.00	1.00	

Table 23. Relative interwell permeability results for the 5 x 4 synthetic field with partially sealing barrier - horizontal wells ($k_{ref} = 100$ mD, $\Delta t_{eq} = 6.59$ days)

	P1	P2	P3	P4	Average
I1	-32	130	64	97	65
I2	321	67	195	96	170
I3	30	93	38	85	62
I4	80	114	89	111	98
I5	119	98	130	115	116
Average	104	101	103	101	

for well pair I01-P01 was negative because the influence function for the pair was calculated using the late time solution. When the interwell connectivity coefficients are small, they are translated to early time-periods and, thus, the late time solution becomes inaccurate. Thus, the negative value was set to zero due to small connectivity coefficient.

4.6. Reservoir with a sealing barrier

Figure 29 shows the top view of the x-direction permeability distribution for the sealing barrier case. The cells in white colour were inactive and thus, served as a seal-

ing barrier. As seen on the figure, the barrier completely divides the reservoir into two compartments. Based on the change in average reservoir pressure calculated from each producer, the compartmentalisation can be inferred.

Table 24 and Figure 30 show the results for the interwell connectivity coefficients. Similar to the previous cases, the results clearly reflect the presence of the sealing barrier. Some connectivity coefficients are very small and even negative. They indicate poor connectivity or no connectivity at all.

Table 25 and Figure 31 present the corresponding

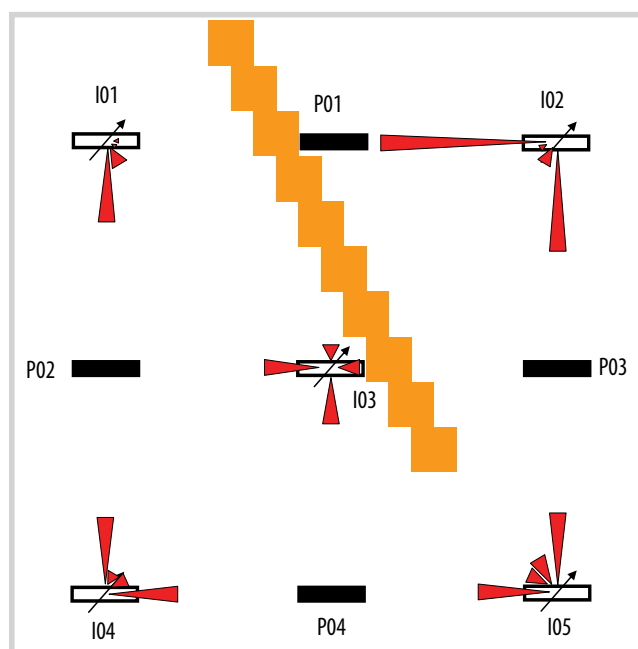


Figure 27. Representation of the connectivity coefficients for the case of 5×4 dual-porosity reservoir with a partially sealing barrier - horizontal wells.

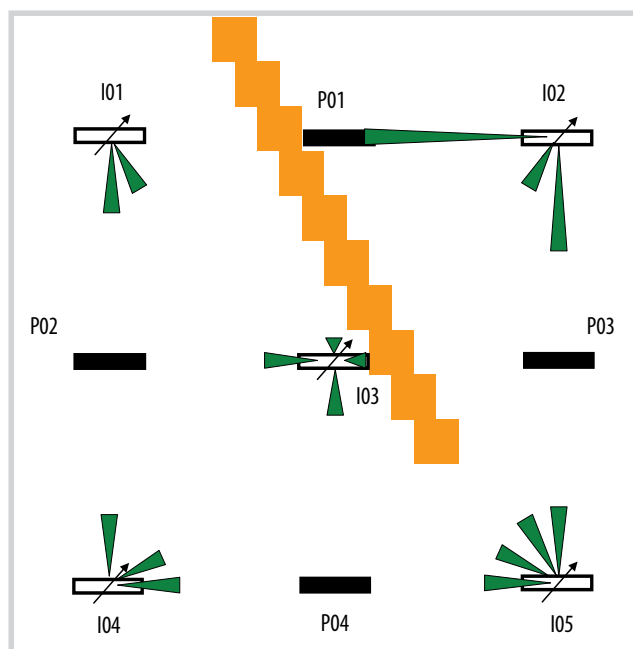


Figure 28. Representation of relative interwell permeability for the case of 5×4 dual-porosity reservoir with a partially sealing barrier - horizontal wells.

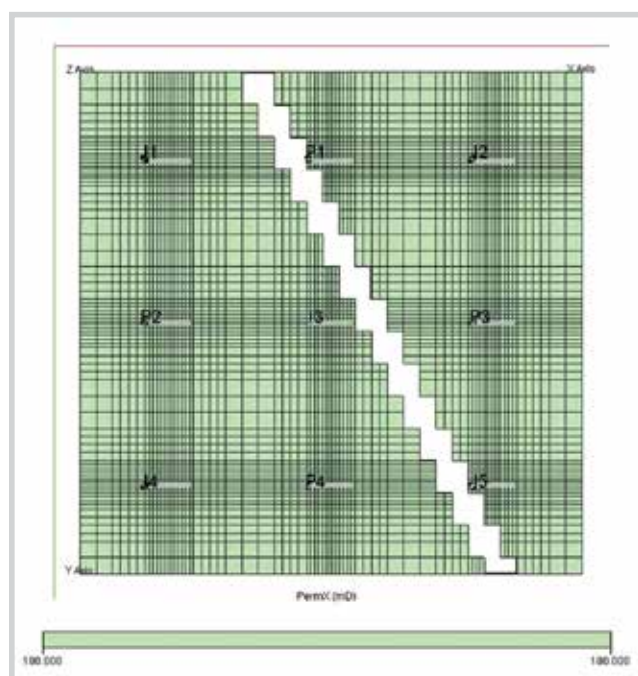


Figure 29. Top view of the simulation model showing the permeability in x direction for the case of 5×4 synthetic field with a sealing barrier - horizontal wells.

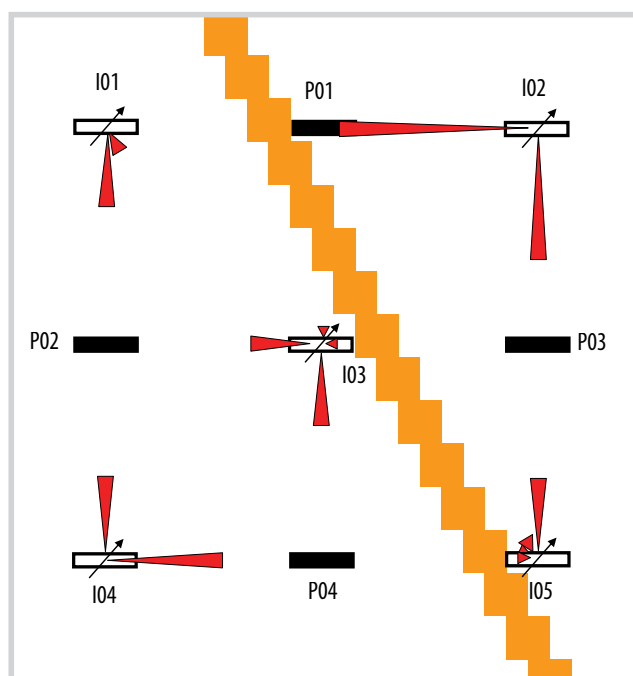


Figure 30. Representation of the connectivity coefficients for the 5×4 synthetic field with a sealing barrier - horizontal wells.

relative interwell permeabilities with the equivalent time of 6.59 days, and the reference permeability of 100 mD. A cut-off coefficient of 0.06 was applied to eliminate the low connectivity coefficients. Thus, the relative interwell permeability corresponding to the coefficients lower than 0.06 were set to zeros. The resulting relative interwell permeabilities show a clear presence of the sealing barrier (Figure 31).

Table 26 shows the results for the average reservoir pressure change for all producers in each representative case described in this section. Similar to the previous section, the changes in average reservoir pressure for all the cases are about the same and close to the simulated pressure changes. For the case with the presence of a sealing barrier, the resulting pressure changes for wells P01 and

Table 24. Interwell connectivity coefficient results from simulation data for the 5 × 4 synthetic field with a sealing barrier - horizontal wells

	P1	P2	P3	P4	Sum
β_{0j} (psia)	-336.6	-266.0	-225.4	-365.7	-1194
I1	0.00	0.35	0.00	0.10	0.45
I2	0.87	-0.01	0.60	-0.01	1.44
I3	0.05	0.27	0.05	0.35	0.73
I4	-0.02	0.36	-0.02	0.53	0.84
I5	0.07	0.04	0.35	0.05	0.51
Sum	0.97	1.01	0.97	1.02	

Table 25. Relative interwell permeability results for the 5 × 4 synthetic field with a sealing barrier - horizontal wells ($k_{ref} = 100$ mD, $\Delta t_{eq} = 6.59$ days)

	P1	P2	P3	P4	Average
I1	0	137	0	104	60
I2	391	0	259	0	163
I3	0	106	0	138	61
I4	0	143	0	222	91
I5	89	0	135	0	56
Average	96	77	79	93	

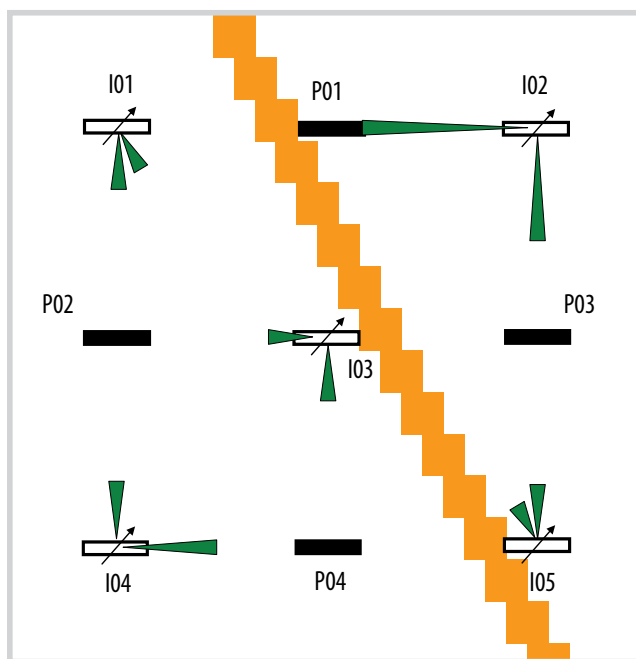


Figure 31. Representation of relative interwell permeability for the 5 × 4 synthetic field with a sealing barrier - horizontal wells.

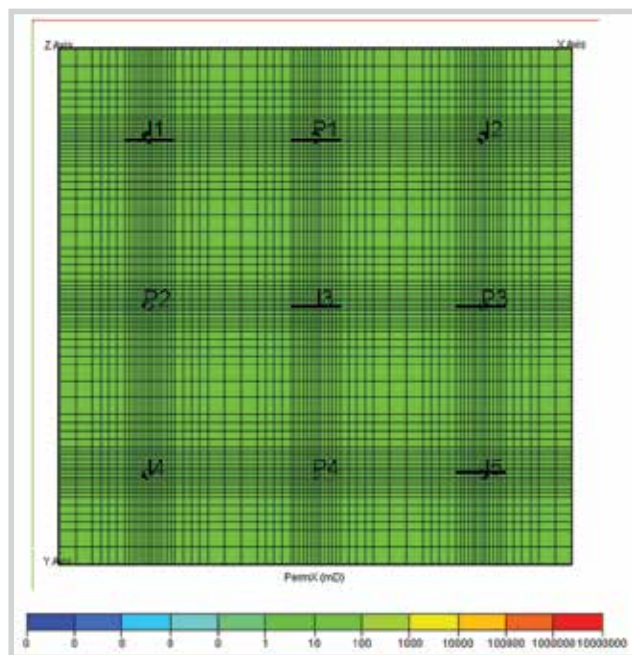


Figure 32. Top view of the simulation model showing the x-direction permeability for the 5 × 4 homogeneous synthetic field - mixed hydraulically fractured and vertical wells.

Table 26. Average pressure change (ΔP_{ave}) after each time interval for different cases of 5 × 4 synthetic field - horizontal wells

Cases	P1	P2	P3	P4
Homogeneous reservoir	285.98	286.04	285.79	285.84
Anisotropic reservoir	285.93	285.92	285.92	285.79
Channel	285.90	285.94	285.82	285.91
Partially sealing barrier	294.99	300.45	296.10	298.96
Sealing barrier	180.93	390.14	180.77	390.18

P03 (about 181 psi) are different from those for wells P02 and P04 (390 psi) indicating two different reservoir compartments. Thus, the reservoir pressure change results are consistent.

5. Results for mixed wellbore conditions

5.1. Mixed case of fully penetrating vertical wells and fully penetrating hydraulic fractures

Figure 32 shows the top view of the permeability dis-

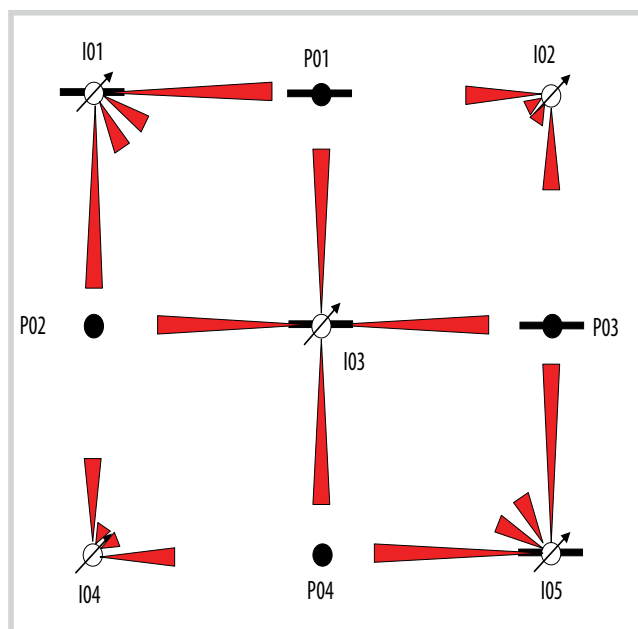


Figure 33. Representation of the connectivity coefficients for the 5 × 4 homogeneous synthetic field - mixed hydraulically fractured and vertical wells.

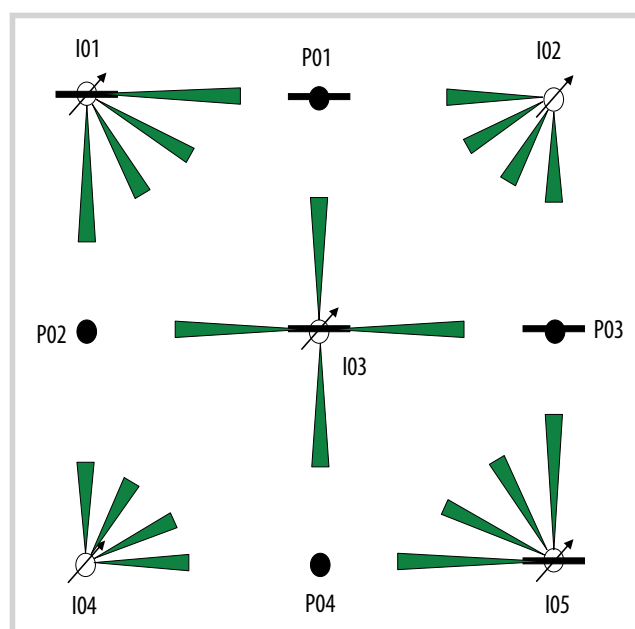


Figure 34. Representation of relative interwell permeability for the 5 × 4 homogeneous synthetic field - mixed hydraulically fractured and vertical wells.

Table 27. Interwell connectivity coefficient results from simulation data for the 5 × 4 homogeneous synthetic field - mixed hydraulically fractured and vertical wells

	P1	P2	P3	P4	Sum
β_{oj} (psia)	-281.1	-502.1	-282.1	-501.9	-1567
I1	0.37	0.36	0.10	0.11	0.94
I2	0.16	0.04	0.16	0.04	0.41
I3	0.32	0.33	0.34	0.33	1.32
I4	0.04	0.16	0.04	0.16	0.41
I5	0.11	0.11	0.35	0.36	0.93
Sum	1.00	1.00	1.00	1.00	

Table 28. Relative interwell permeability results for the 5 × 4 homogeneous synthetic field - mixed hydraulically fractured and vertical wells ($k_{ref} = 100$ mD, $\Delta t_{eq} = 7.33$ days)

	P1	P2	P3	P4	Average
I1	123	122	92	93	108
I2	81	74	80	74	77
I3	109	110	114	110	111
I4	75	81	74	80	78
I5	93	94	121	125	108
Average	96	96	96	97	

tribution for this case. As shown on the figure, wells I01, P01, I03, P03 and I05 are hydraulically fractured wells and all the other wells are fully penetrating vertical wells. Table 27 and Figure 33 present the interwell connectivity coefficient results for this case. It is obvious that hydraulically fractured injectors have better connectivity with the producers than the vertical injectors.

Table 28 and Figure 34 show the corresponding relative interwell permeability results for this reservoir. The relative permeabilities for the well pairs of vertical injectors are slightly lower than those of hydraulic fractures. However, the calculated relative interwell permeability

is in good agreement with the input permeability for the model of 100 mD.

Figure 35 shows the comparison of the interwell connectivity coefficients results obtained from simulation data and calculations using influence functions. The coefficients are in good agreement with $R^2 = 0.9875$.

5.2. Mixed case of fully penetrating vertical wells and horizontal wells

Figure 36 shows the top view of the permeability distribution for this case. As shown on the figure, wells I01, P01, I03, P03 and I05 are horizontal wells and all the other

wells are vertical wells. Figure 37 shows the cross section through wells I04, P04 and I05. Wells I04 and P04 are fully penetrating vertical wells and similar to other horizontal wells, and horizontal well I05 is completed in the middle layer.

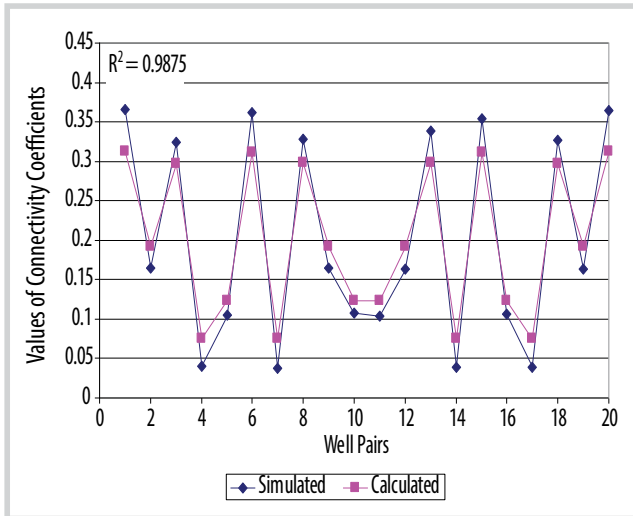


Figure 35. Comparison of the interwell connectivity coefficient results for the 5 × 4 homogeneous synthetic field - mixed hydraulically fractured and vertical wells.

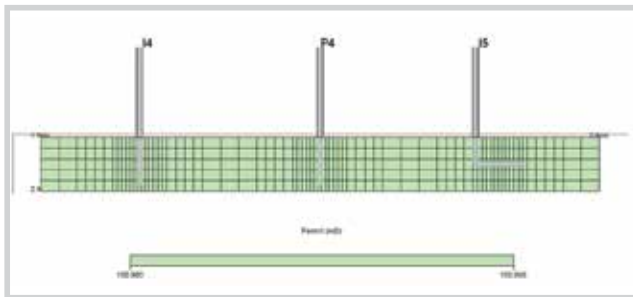


Figure 37. Cross sectional view showing three wells of the 5 × 4 homogeneous synthetic field - mixed horizontal and vertical wells.

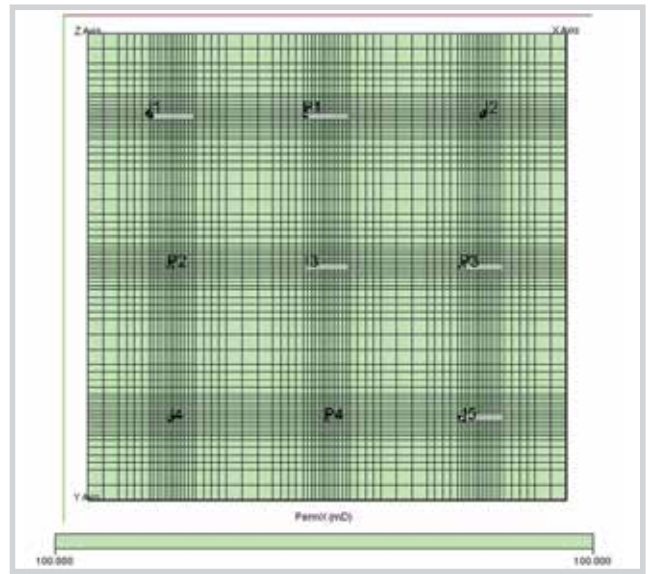


Figure 36. Top view of the simulation model showing the x direction permeability for the 5 × 4 homogeneous synthetic field - mixed horizontal and vertical wells.

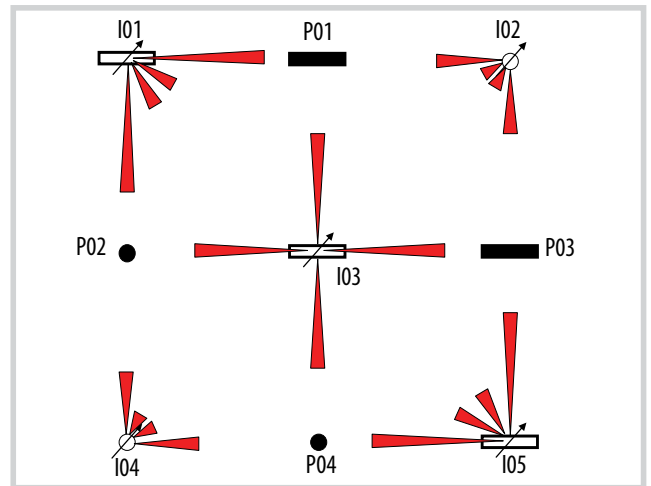


Figure 38. Representation of the connectivity coefficients for the 5 × 4 homogeneous synthetic field - mixed horizontal and vertical wells.

Table 29. Interwell connectivity coefficient results from simulation data for the 5 × 4 homogeneous synthetic field - mixed horizontal and vertical wells.

	P1	P2	P3	P4	Sum
β_{oj} (psia)	-349.3	-540.1	-350.7	-540.5	-1781
I1	0.34	0.35	0.12	0.14	0.94
I2	0.17	0.06	0.17	0.06	0.47
I3	0.30	0.29	0.31	0.30	1.20
I4	0.06	0.17	0.06	0.17	0.46
I5	0.13	0.13	0.33	0.34	0.93
Sum	1.00	1.00	1.00	1.00	

Table 30. Relative interwell permeability results for the 5 × 4 homogeneous synthetic field - mixed horizontal and vertical wells ($k_{ref} = 100$ mD, $\Delta t_{eq} = 7.33$ days)

	P1	P2	P3	P4	Average
I1	117	122	96	102	109
I2	80	80	82	83	81
I3	107	104	111	106	107
I4	83	79	82	78	81
I5	100	100	116	118	108
Average	97	97	97	97	

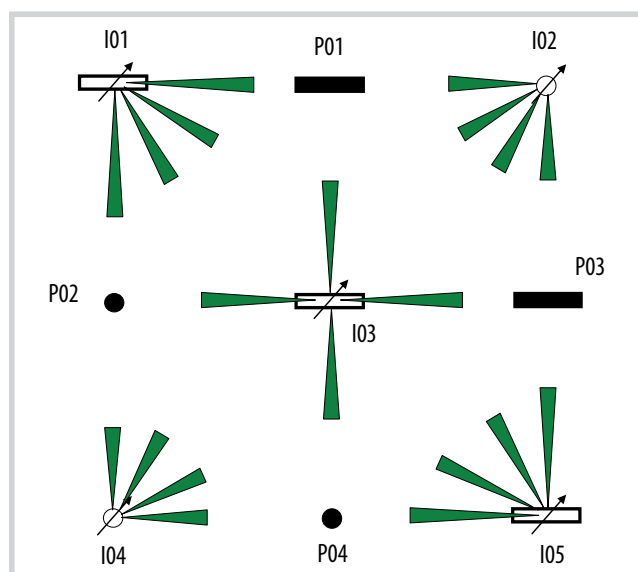


Figure 39. Representation of relative interwell permeability for the 5 × 4 homogeneous synthetic field - mixed horizontal and vertical wells.

Table 29 and Figure 38 present the interwell connectivity coefficient results for this case. It is obvious that horizontal injectors have better connectivity with the producers than the vertical injector. Table 30 and Figure 39 show the corresponding relative interwell permeability results for this reservoir. The relative permeabilities for the pairs of vertical injectors are slightly lower than those of horizontal injectors. This could be due to numerical errors and analytical assumptions. However, the calculated relative interwell permeability is in good agreement with the input permeability for the model of 100 mD. Figure 40 shows the comparison of the interwell connectivity coefficients results obtained from simulation data and by calculation using influence functions. The coefficient results are in good agreement with $R^2 = 0.9681$.

6. Conclusions and recommendations

- The interwell connectivity determination technique can be applied to reservoirs even when the wells are hydraulically fractured;
- The effect of a vertically fractured well on other wells at far distance is very close to the effect of its vertical well counterpart given the same flow rate. Thus, only the pressure drops at the wells themselves are different;
- The interwell connectivity determination technique can be applied to reservoirs containing horizontal wells;
- The well length at the observations wells or the well directions do not affect the interwell connectivity results;

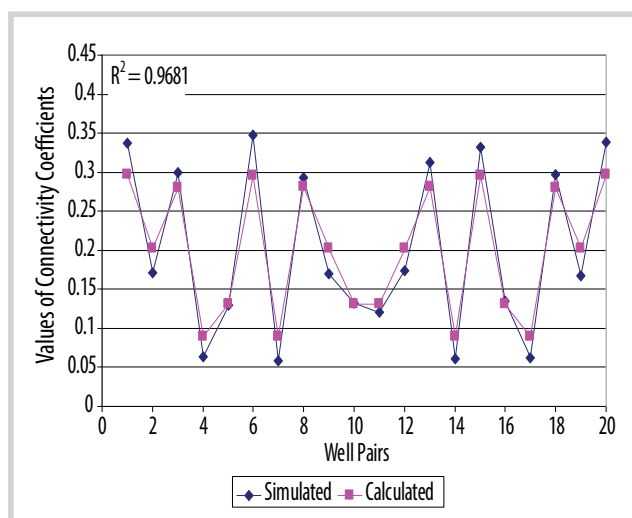


Figure 40. Comparison of the simulated and calculated interwell connectivity coefficient results for the 5 × 4 homogeneous synthetic field - mixed horizontal and vertical wells.

- The complication of pressure distribution caused by a horizontal well can be captured using the analytical model and thus its connectivities with other wells can be interpreted and quantified.
- The results obtained from the mixed wellbore condition cases showed that connectivities between wells with different and complicated wellbore conditions in a reservoir can be inferred using the bottomhole pressure fluctuation technique knowing the shape factors of the wells.

References

- [1] Alejandro Albertoni and Larry W. Lake, "Inferring interwell connectivity only from well-rate fluctuations in waterfloods", *SPE Reservoir Evaluation and Engineering Journal*, Vol. 6, No. 1, pp. 6 - 16, 2003. DOI: 10.2118/83381-PA.
- [2] Alejandro Albertoni, "Inferring interwell connectivity from well-rate fluctuations in waterfloods", The University of Texas at Austin, 2002.
- [3] Belkis Teresa Refunjol, "Reservoir characterization of North Buck Draw field based on tracer response and production/injection analysis", M.S. Thesis, The University of Texas at Austin, 1996.
- [4] Ali Al-Yousef, "Investigating statistical techniques to infer interwell connectivity from production and injection rate fluctuations", PhD Dissertation. University of Texas at Austin, 2006.
- [5] Ali A. Yousef, Pablo Hugo Gentil, Jerry L. Jensen, and Larry W. Lake, "A capacitance model to infer interwell

connectivity from production and injection rate fluctuations", *SPE Reservoir Evaluation & Engineering*, Vol. 9, No. 6, pp. 630 - 646, 2006. DOI: 10.2118/95322-PA.

[6] Djebbar Tiab, "Inferring interwell connectivity from well bottom hole pressure fluctuations in waterfloods", *SPE Production and Operations Symposium, Oklahoma, USA, 31 March - 3 April 2007*. DOI: 10.2118/106881-MS.

[7] Djebbar Tiab and Dinh Viet Anh, "Inferring interwell connectivity from well bottom hole pressure fluctuations in waterfloods", *SPE Reservoir Evaluation & Engineering*, Vol. 11, No. 5, pp. 874 - 881. DOI: 10.2118/106881-PA.

[8] Dinh Viet Anh and Djebbar Tiab, "Interpretation of interwell connectivity tests in a waterflood system", *SPE Annual Technical Conference and Exhibition, Denver, Colorado, USA, 21 - 24 September, 2008*.

[9] Dinh Viet Anh, "Interwell connectivity tests in waterflood systems", PhD Dissertation, University of Oklahoma, 2009.

[10] Taufan Marhaendrajana, "Modeling and analysis of flow behavior in single and multiwell bounded reservoirs", PhD Dissertation, Texas A&M University, 1999.

[11] T. Marhaendrajana, N.J. Kaczorowski, and T.A. Blasingame, "Analysis and interpretation of well test

performance at Arun field, Indonesia", *SPE Annual Technical Conference and Exhibition, Houston, Texas, 3 - 6 October, 1999*. DOI: 10.2118/56487-MS.

[12] D.N. Dietz, "Determination of average reservoir pressure from build-up survey", *JPT*, Vol. 17, No. 8, pp. 955 - 959, 1965. DOI: 10.2118/1156-PA.

[13] E. Ozkan, "Performance of horizontal wells", PhD Dissertation, University of Tulsa, 1988.

[14] Alain C. Gringarten, Henry J. Ramey Jr., and R. Raghavan, "Unsteady-state pressure distributions created by a well with a single infinite-conductivity vertical fracture", *Society of Petroleum Engineers Journal*, Vol. 14, No. 4, pp. 347 - 360, 1974. DOI: 10.2118/4051-PA.

[15] Schlumberger, "ECLIPSE 100 black oil simulator" (version 2006.1), 2006.

[16] Heber Cinco-Ley and Fernando Samaniego-V, "Transient pressure analysis for fractured wells", *JPT*, Vol. 33, No. 9, pp. 1749 - 1766, 1981. DOI: 10.2118/7490-PA.

[17] Djebbar Tiab, "Analysis of pressure derivative without type-curve matching: Vertically fractured wells in closed systems", *Journal of Petroleum Science and Engineering*, Vol. 11, No. 4, pp. 323 - 333, 1994. DOI: 10.1016/0920-4105(94)90050-7.